PHOTODEGRADATION OF PYROGENIC DISSOLVED ORGANIC MATTER (*PY*-DOM): A COMBINED PHOTON COUNTING AND DISTRIBUTION-BASED FT-ICR MS STUDY

by

BURKE C. LEONCE

Bachelor of Science, 2010
Troy University
Troy, Alabama

Submitted to the Graduate Faculty of the
College of Science and Engineering
Texas Christian University
in partial fulfilment of the requirements for the degree of

Master of Science

May 2017

PHOTODEGRADATION OF PYROGENIC DISSOLVED ORGANIC MATTER (*PY*-DOM): A COMBINED PHOTON COUNTING AND DISTRIBUTION-BASED FT-ICR MS STUDY

by:

Burke Leonce

Thesis approved:

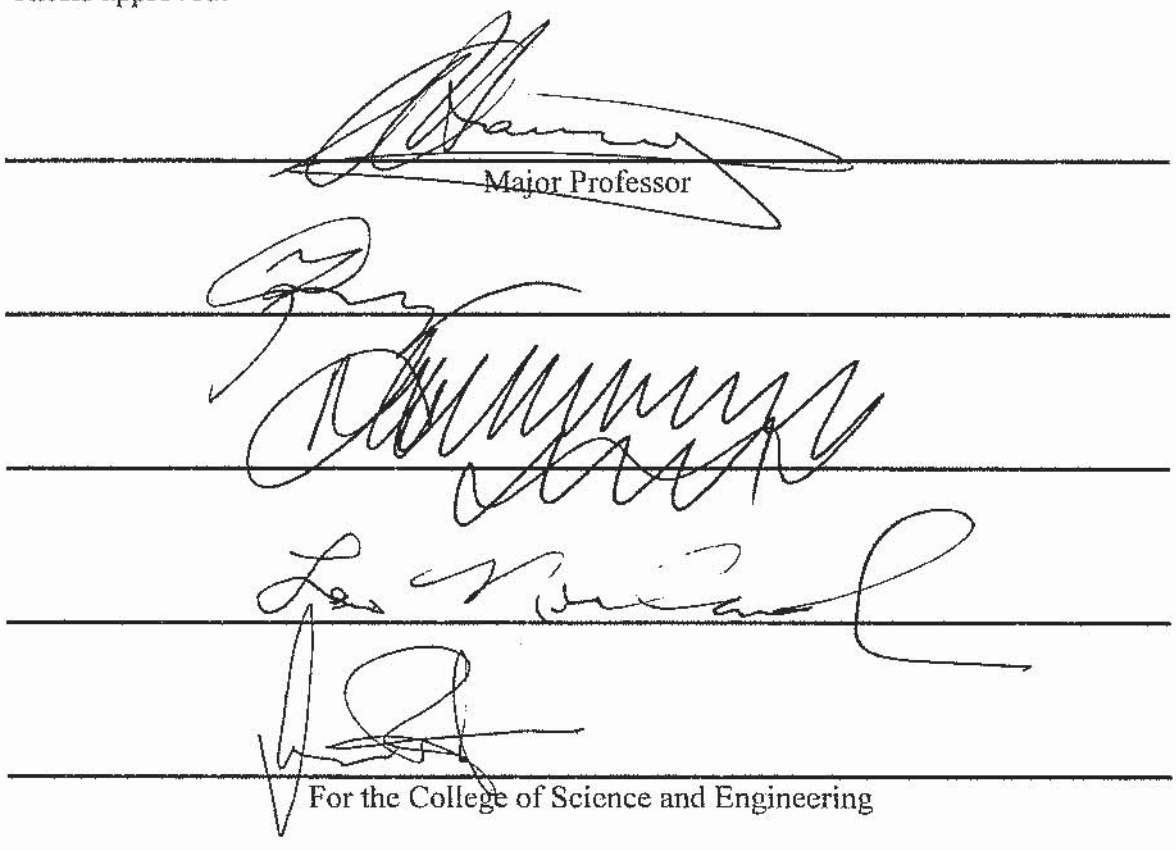

Major Professor

For the College of Science and Engineering

ACKNOWLEDGEMENTS

I am grateful for the counsel and support of my committee members who always lifted my spirits with a well-timed quip, albeit unknowingly. Give thanks for the boss, Dr. Omar Harvey, who knew I would complete this thesis despite my intermittent bouts of insecurity. As an advisor, you instilled in me the necessary skills required to be a professional scientist. More importantly, as a mentor, your unwavering requirement of excellence in every facet of life is the most valuable lesson I learned as a graduate student. Thank you, Dr. Zygmunt Gryczynski for sharing your boundless wisdom in the field of time-resolved fluorescence spectroscopy. Thank you, Dr. Slattery, for your cheerful insight during our committee meetings. And thank you Dr. Leo Newland for your critical analysis of my research methodology and results.

I am forever indebted to Patrick Lazzarino and the other members of our tiny, but productive, research group for both physical and moral support during the darkest of times. Dr. Harvey promised that this thesis would be an iterative process; the umpteenth trial would not be successful without you. I would also like to thank Zhanatay, Hung and Sangram for providing a space for me to work in your lab and Robert Denkhaus for assisting with sampling at the Fort Worth Nature Center. Notably, the ultra-high resolution mass spectrometry section of this thesis would not be possible without the fervent support of Dr. Yina Liu and Dr. Li-Jung Kuo from the Environmental Molecular Sciences Laboratory, (Richland, Wa.) of the Pacific Northwest National Laboratory, (Sequim, Wa.).

Finally, the utmost gratitude and respect is reserved for my family – my wife and my mother – for their abundant patience, love and honesty, short of which, I would not have completed this thesis.

TABLE OF CONTENTS

LIST OF FIGURES

LIST OF TABLES

LITERATURE REVIEW

Pyrogenic organic matter (*Py*-OM) produced from the incomplete combustion of organic material, consists of an insoluble particulate fraction (*pPy*-OM) and a soluble (*Py*-DOM) fraction. The particulate fraction of *Py*-OM has been widely studied,[1-4] however, estimates of the contribution of pyrogenic dissolved organic matter (*Py*-DOM) to global carbon flux has remained elusive due to significant knowledge gaps within the terrestrial aquatic dissolved organic matter (DOM) pool. Kim et al.[5] provided the first definitive evidence of *Py*-DOM in terrestrial waters using ultra-high resolution mass spectrometry; fifty percent of DOM isolated from the fire-impacted Rio Negro branch of the Amazon River were identified as having a hydrogen-deficient molecular signature characteristic of thermally altered vegetative matter. Since then, global estimates conclude that roughly 10% of the 250 mega-metric tons of DOM in riverine systems is derived from thermally altered organic material.[6] Furthermore, a projected 62% increase in wildfire activity is expected in mid- to high-latitude regions.[7] Thus, quantitative systematic studies are needed to elucidate both the short and long-term environmental implications of increasing fire sizes and the *Py*-DOM inputs associated with this change.

Numerous studies have attempted to characterize *Py*-DOM from natural sources,[5, 8-12] however, few focus on feedstock and pyrolysis temperature effects on *Py*-DOM molecular structure.[13-15] Nonetheless, some insight into molecular structure and functional group variation of *Py*-DOM obtained from a range of charred organic material can be gained from recent studies. Uchimaya et al.[15] compared proportions of base extractable *Py*-DOM components from five pyrolyzed carbonaceous materials using fluorescence excitation-emission mapping (EEM) spectrophotometry coupled with parallel factor analysis (PARAFAC). The proportion of fulvic-like component generally increased with increasing pyrolysis temperature (350 ^{o}C/400 ^{o}C, 500 ^{o}C, 650 ^{o}C, 800 ^{o}C) to a maximum at 650 ^{o}C. In contrast, the proportion of a high molecular

weight humic-like component generally decreased with increasing temperature. Interestingly, a low molecular weight humic-like component was consistently identified at all pyrolysis temperatures except 500 ºC *Py*-DOM – only lignin derived *Py*-DOM contained this component.

In a separate study, Lin et al.[16] identified higher proportions of low molecular weight neutrals in water extracts of sawdust pyrolyzed at 450 ºC (45%) and 550 ºC (37%). Additionally, lower temperature extracts contained four times the proportion of humics present in higher temperature extracts (16 % versus 4%), and fourteen times the proportion of lower molecular weight acids (42% versus 3%). Extracts from lower temperature *Py*-DOM was also more aromatic (4.8 versus 2.2), contained twice the proportion of biopolymers (13.7% versus 7.7%), and was 22 times more concentrated than higher temperature extracts (93412 ppb-OM versus 4285 ppb-OM).

It is widely accepted that thermal conversion of lignocellulose drives the characteristics of *Py*-DOM derived from herbaceous materials.[2, 15, 17-19] Smith et al.[20] observed a decrease in water soluble extracts from cellulose and lignin-derived *Py*-OM with increasing temperature (300 ºC, 400 ºC and 500 ºC). The composition of these extracts however varied widely between materials and pyrolysis temperature. While the carboxylic acid content was similar for both materials, carbohydrates were only observed in cellulose. Cellulose also contained relatively fewer phenols and polycyclic aromatic hydrocarbons (PAHs) than lignin. As pyrolysis temperature increased the number of acids, phenols and carbohydrates identified in cellulose-derived extracts decreased. In lignin material, phenols and acids identified decreased whereas PAHs remained constant. During pyrolysis, thermal conversion of lignin and cellulose occurs at different rates producing a heterogeneous suite of products and intermediates, hence structural classification of *Py*-DOM along a gradient remains ill-defined.

The solubility and hence mobility of *Py*-DOM is largely attributable to abiotic and biotic oxidation of aromatic ring structures which in turn depends on the chemical structure of *Py*-OM.[5, 21] As the aromaticity of *Py*-DOM increases with residence time it becomes increasingly susceptible to UV radiation. Stubbins et al.[22] quantified the photo-lability of marine *Py*-DOM by examining the difference in benzenepolycarboxylic acid (BPCA) oxidation products before and after exposure to artificial irradiation. Photodegradation of *Py*-DOM occurred more rapidly than its unburnt parent material and was attributable mainly to a higher proportion of highly condensed aromatics. Approximately 20% of *Py*-DOM was degraded after two days with 95% of initial *Py*-DOM being lost after 28 days. Despite these findings, the rates at which this breakdown occurs, how it occurs and the factors influencing that photodegradation has not been elucidated.

Photodegradation of *Py*-DOM is the major contributing factor to the breakdown of highly condensed aromatics into the more labile compounds favored by microbes.[22] Oxidation (be it abiotic or biotic) of aromatic structures results in by-products that are more water-soluble and biologically labile providing energy and carbon for microbes in aquatic ecosystems.[23] Kim et al.[23] examined the changes in DOM molecular composition induced by microbial decomposition from two forested streams using ultra-high resolution mass spectrometry. Microbes preferentially degraded compounds with a higher O:C ratio; however, *Py*-DOM was more resistant to microbial degradation than unaltered DOM. Although the age and structure of this refractory carbon was undetermined, Abiven et al.[24] noted a 40-55-fold increase in oxidized by-products of condensed aromatic structures released from 10-year old char as opposed to fresh char. Therefore, time is an important factor in determining the nature and properties of *Py*-DOM, and its microbial degradability. In addition Ward et al.[25] noted the preferential partial photo-oxidation of *Py*-DOM versus DOM, yielding photoproducts of higher O/C ratio than the parent compound.

Approximately 68-91% of carbon in *Py*-DOM was partially oxidized by sunlight, thus highlighting the importance of photodegradation in the direct mineralization of *Py*-DOM and as a critical step in the production of microbially favored substrates.

The rate of photodegradation of DOM and *Py*-DOM in terrestrial aquatic systems is contingent on variation in chemical structure.[9, 25] In this study, the chemical structure of DOM and *Py*-DOM extracted from grass and wood material was investigated using fluorescence lifetime spectroscopy and ultra-high resolution mass spectrometry. The bulk rate of photodegradation of DOM/*Py*-DOM and the contributing components to that photodegradation, was also investigated using systematic changes in fluorescence behavior. Results of this study will provide new insights into the transformation and mobility DOM/*Py*-DOM in terrestrial aquatic systems and the environmental implications of an increased input of fire-altered DOM.

CHAPTER I

CHARACTERISTICS OF PYROGENIC DISSOLVED ORGANIC MATTER (*PY*-DOM) AS ELUCIDATED THROUGH COMBINED PHOTON COUNTING AND ULTRA-HIGH RESOLUTION MASS SPECTROMETRY ANALYSES

Introduction

The average size of US wildfires has tripled over the past two decades (1995-2015) with a record 4.1 million total hectares burned by wildfires in 2015 (Fig. 1),[26] producing roughly 20 Megatons (1.8×10^{10} kg) of pyrogenic organic matter (*Py*-OM).[27] This *Py*-OM has an insoluble particulate fraction (*pPy*-OM) and a soluble (*Py*-DOM) fraction. Particulate *Py*-OM is largely degraded in situ, however the dissolved component (*Py*-DOM) is mobile[24] and subject to both abiotic (e.g. photodegradation and chemical oxidation) and biotic (e.g. microbial incorporation and respiration) reaction processes.[28-30] Work by Abiven et al.[24] suggests only minimal chemical modification of *Py*-DOM occurs in soil, however, recent estimates suggest that less than 50% of the 4 Megatons of *Py*-DOM entering US rivers and streams in 2015 will likely reach the ocean.[1, 6] The fact that only 50% of *Py*-DOM is expected to reach the ocean points to an unidentified riverine sink and/or significant aquatic transformation of *Py*-DOM during its transport.

Chemical and structural variation in fire-altered organic material versus its unburnt counterpart[8] suggest that the potential stability and interactions of *Py*-DOM in freshwater systems may be dominated by very different mechanisms than that of DOM. However, research focused on feedstock and pyrolysis temperature effects on *Py*-DOM molecular structure[13-15] is still in its infancy. For example, a decrease in proportion of humics, low molecular weight acids, biopolymers, aromaticity and concentration with increasing pyrolysis temperature has been observed in water extractable DOM.[16] In addition, thermal degradation of lignocellulose alters

molecular structure and functional group chemistry (e.g. phenolic, carboxylic etc.)[20] producing a dynamic suite of products and intermediates, thus molecular characterization of *Py*-DOM remains indefinable.

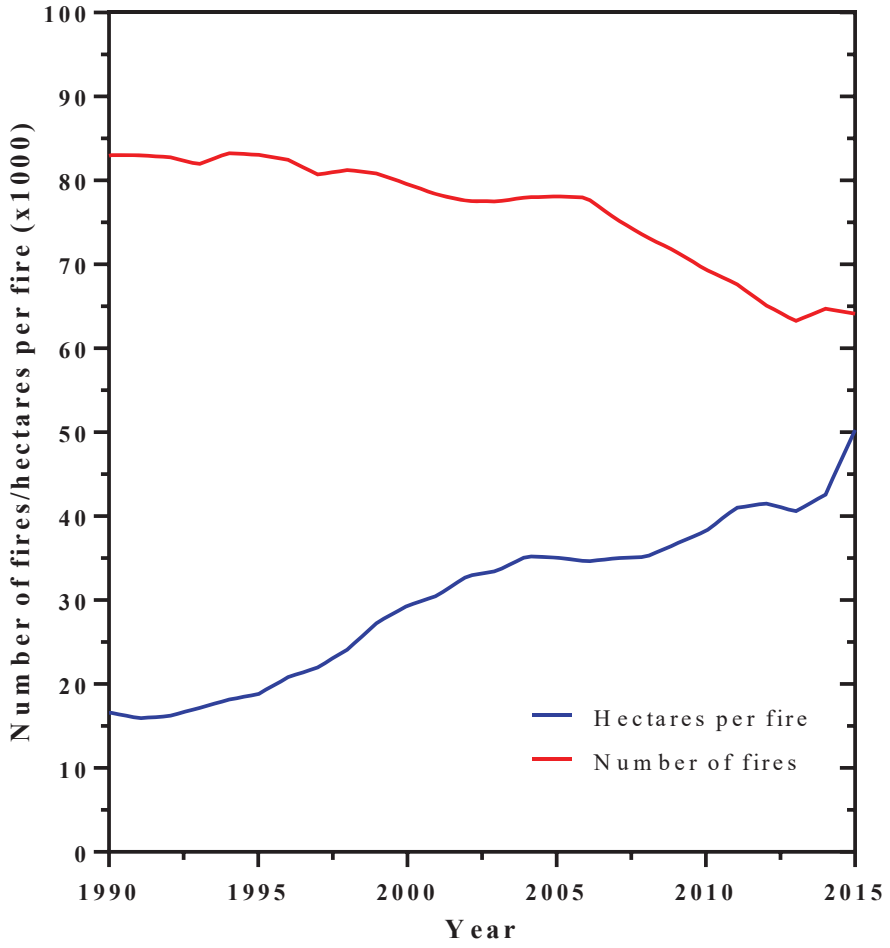

Figure 1. Recent trends in the number and average size of wildfires between 1990 and 2015.[26]

Full characterization of *Py*-DOM has remained elusive due to inadequate resolution of DOM using current methods. Techniques such as Carbon Nuclear Magnetic Resonance (C-NMR) spectroscopy,[12, 31] provide bulk functional group characteristics (carboxylic acids, aliphatic chains) of DOM, however they cannot solely identify particular compounds within its structure.[32] And while Gas Chromatography Mass Spectrometry (GC-MS) has been utilized to

examine *Py*-DOM,[33] humic fragments require pyrolytic/chemolytic treatments prior to analysis,[34] due to their large size (> 500 Da) and polarity, thus limiting molecular structure/weight characterization.[32, 35] The ultra-high resolution of Fourier transform ion cyclotron resonance mass spectrometry (FT-ICR MS) is ideal for resolving molecular level composition of complex macromolecules such as DOM[36] and has provided a wealth of new insights into the molecular level characterization of *Py*-DOM.[20, 25, 37] However few studies have investigated pyrolysis temperature dependent variation in *Py*-DOM.[20] In addition, fluorescence spectroscopy, (particularly excitation emission matrix; EEM) is widely used for characterizing organic matter and provides a bulk view of fluorescence properties of components present within a particular spectral range[38]. While EEM has been widely used, fluorescence lifetime measurements are not prevalent, and have never been used in studies of *Py*-DOM. I utilized Time resolved fluorescence spectroscopy (lifetime measurements) to identify the chromophoric components contributing to fluorescence character of DOM. Lifetime measurements i.e. time-correlated single photon counting (TCSPC) is particularly advantageous over steady state measurements due to its insensitivity to conditions such as scattering, fluorophore concentration and turbidity.[39] In addition, fluorescence lifetime measurements are ideal for resolving broad featureless spectra characteristic of DOM.[39-40]

In this study, the chemical structure of solid phase extract DOM (SPE-DOM) and *Py*-DOM (base-extractable fraction) extracted from grass and wood material pyrolyzed at 300 ºC and 400 ºC was investigated using TCSPC and FT-ICR MS. These techniques represent the analytical zenith of DOM, and to our knowledge this is the first study to utilize these techniques concurrently. The objective of this study was to provide molecular level characterization of the soluble fraction from charred and uncharred herbaceous feedstock to gain insight into potential ecosystem-reaction mechanisms of this increasing influx of fire-altered organic material.

Materials and Methods

Preparation of charcoals and extraction of Py-DOM

Charcoals were produced from Switchgrass (*Panicum virgarum*) and Eastern Cedar (*Juniperus virginiana*) sampled from the Fort Worth Nature Center (Fort Worth, TX, USA) in May 2016. Plant material was collected by hand and chosen due to the variation in vascular tissue and taxonomy [Switchgrass (angiosperm, non-woody, C4), Eastern red cedar (gymnosperm, woody, C3)]. In the laboratory, Switchgrass root was removed and samples were air dried for 24 hours. Subsequently, plant materials were cut into 1 inch pieces and oven dried at 80 °C for 24 hours. Samples were then tightly packed into ceramic crucibles; crucibles were tightly wrapped in aluminum foil (to produce oxygen-limited conditions) and then charred in a Temco Type 1500 laboratory furnace (Thermo Electric, Dubuque, IA). Charring was from room temperature to the target pyrolysis temperatures of 300 °C or 400 °C at a ramp rate of 20-25 °C/min and kept at target pyrolysis temperature for 1 h. After the 1 h pyrolysis period the oven was kept closed and allowed to cool to room temperature before the resulting charcoals were removed. Charcoals were then ground, sieved (250 μm) and stored in air-tight glass jars at room temperature.

Extraction of *Py*-DOM from the charcoals followed the operationally-defined separation of soil organic matter into humic substances (humin, humic acid, and fulvic acid) based on solubility across different pH ranges.[41] In this approach, humin is operationally-defined as being insoluble across the pH scale, fulvic acid (FA) as being soluble across the entire pH range, and humic acid (HA) as being base-, but not acid-soluble.[42] Studies on DOM in the environment focus exclusively on the HA and FA fractions of organic matter. As such, both the HA and FA fractions were targeted in extracting *Py*-DOM from the charcoals. Between 1 and 2 g of charcoal were weighed into 50-mL centrifuge tubes and 40 mL of 0.1M NaOH added to make a charcoal-

NaOH suspension. Charcoal-NaOH suspensions were shaken end-over-end on a rotational shaker for 24 h at room temperature, filtered (P8 filter paper; ThermoScientific,Waltham, MA), and the resulting *Py*-DOM-containing extract adjusted to pH 5 with 0.1 N HCl. This extract served as the stock solution for fluorescence. Extract pH was determined using a AB250 benchtop meter (ThermoScientific, Waltham, MA) and was chosen to be in line with rainfall pH across the conterminous United States (4.9-6.4; Fig. 2).[43] *Py*-DOM nomenclature was referenced by parent material abbreviation and pyrolysis temperature, thus Eastern Cedar and Switchgrass pyrolyzed a 300ºC was referenced as EC300 and SG300 respectively.

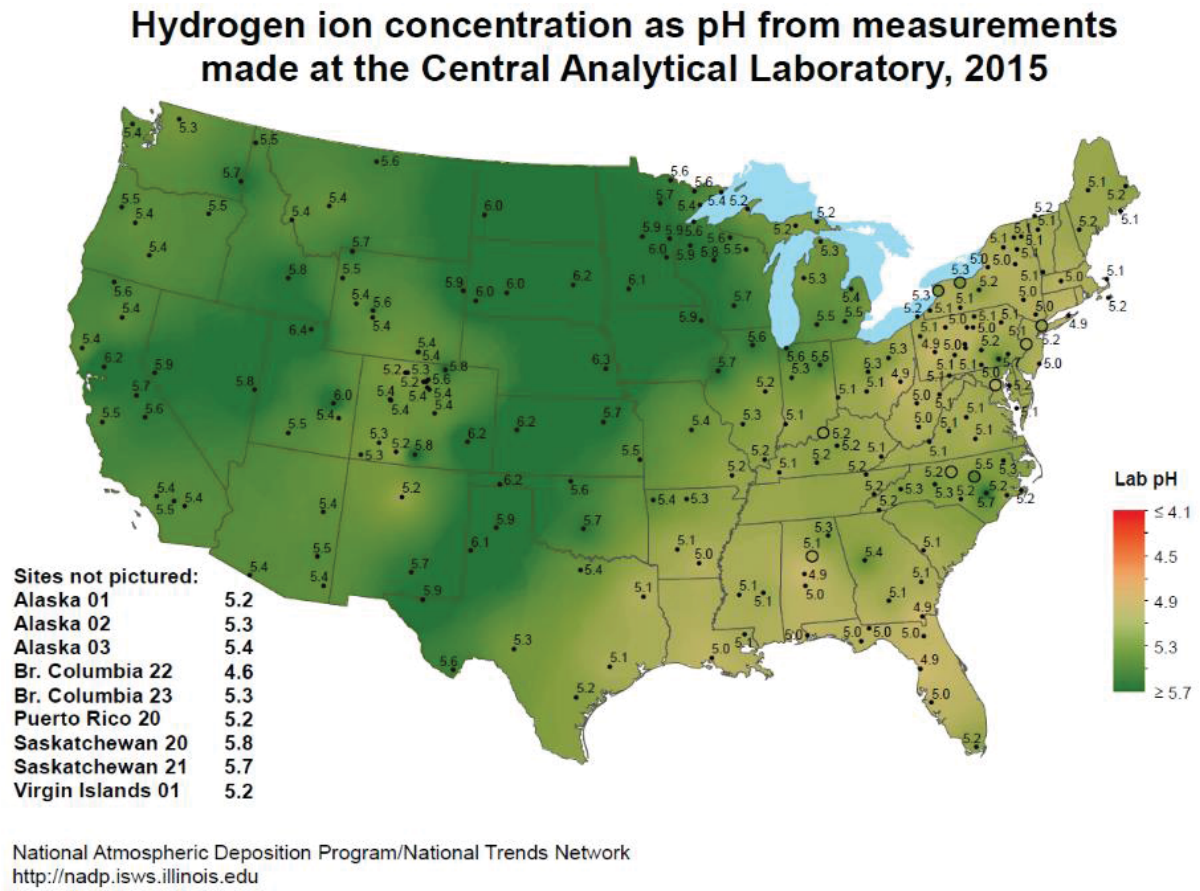

Figure 2. Map showing the pH of rainfall across the conterminous United States in 2015.[43]

Fluorescence spectra collection and time-resolved fluorescence spectroscopy

Fluorescence emission spectra for each sample were collected in a 1 cm path length cuvette. All sample absorbances at UV_{365} were 0.20 ± 0.01 except EC400 which was 0.07 (Evolution 220 UV-vis spectrophotometer; ThermoScientific,Waltham, MA). Fluorescence emission spectra for each sample were collected at an excitation wavelength of 405 nm and emission spectra observed between 430 nm and 700 nm (Varian Cary Eclipse fluorescence spectrophotometer). The fluorescence emission spectra for the 0.1 M NaOH solution was also collected with the sample and used to correct the sample spectra for Raman scattering effects. Steady state fluorescence spectra were used to determine suitable excitation and observation parameters for the lifetime measurements. Fluorescence lifetime was measured on a FluoTime 300 fluorometer (PicoQuant, Inc.) using a 405 nm diode laser. The fluorometer was equipped with an ultrafast microchannel plate photomultiplier detector (MCPPMT) from Hamamatsu, Inc. The fluorescence lifetimes were measured in the magic angle (54.70) condition and data analyzed using FluoFit4 program from PicoQuant, Inc (Germany) using multi-exponential fitting model;

$$I(t) = \sum_i \alpha_i e^{-t/\tau_i} \qquad (1)$$

where, α_i is the amplitude of the decay of the i^{th} component at time t and τ^i is the lifetime of the i^{th} component. The intensity weighted average lifetime (τ_{avg}) were calculated using following equation;

$$\tau_{avg} = \sum_i f_i \tau_i \quad \text{where} \quad f_i = \frac{\alpha_i \tau_i}{\sum_i \alpha_i \tau_i} \qquad (2)$$

FT-ICR MS analysis

Stock solution of extracted DOM was acidified to pH ~ 2, and then passed through Bond Elut PPL cartridges as described in Dittmar el al. 2008.[44] DOM adsorbed on the PPL cartridges were then eluted with 100% HPLC Optima grade methanol (MeOH).[44] Extracted samples were further diluted to a final concentration of 20 mg L^{-1}- C in MeOH for FT-ICR MS analysis.

The SPE-DOM samples were directly infused (3.0 µL/min) into a Bruker 12T Tesla Bruker SolariX FT-ICR MS equipped with electrospray ionization source, and operated in negative mode (ESI-) (Bruker daltonics Inc, Billerica, MA, USA). Spectrum for each sample was collected at 400,000 resolving power (m/Δm50% at m/z 400), and averaged over 200 individual scans. The mass error after internal calibration was < 0.3 ppm. Elemental formulas were assigned to the calibrated masses using an in-house software based on the automated Compound Identification Algorithm described in Kujawinski and Behn,[45] with an assignment tolerance of 1 ppm. It should be noted that feature intensities observed with FT-ICR-MS cannot be directly equated to absolute concentrations.[46] Therefore, samples analyzed with FT-ICR MS were examined based on presence/absence of detected features in each sample.

Data analysis

FT-ICR MS spectra were analyzed as a distribution revealing quantitative bulk characteristics that were otherwise unrecognizable from individual peak analysis. Only signals corresponding to carbon number (C#), atomic H/C ratio (H/C), atomic O/C ratio (O/C) and molecular weight (MW) were used in this study. Spectra signal for C#, H/C, O/C and MW was normalized to the highest signal and sorted in ascending order. Signal distributions were binned at selected intervals. (e.g. O/C ratio signal amplitudes were binned at every 0.1 incremental increase) then fitted using a cubic spline model in GraphPad Prism (version 6). The model was baseline corrected using the linear function in Omnic 8.0 software (ThermoScientific, Waltham,

MA.). Distribution curves were deconvoluted using peak analyzer function in OriginPro (Northampton, MA), fitted using a Gaussian model and component peaks were identified using 2nd derivative function. Goodness of fit was estimated by the agreement of the original peak and peak fit of components. Component peak center and standard deviation was equivalent to the mean value (± SD), with area under peak representing proportion of mean value contributing to total signal. Only component peak centers representing more than 10% of total signal were plotted.

Results and Discussion

Insights from fluorescence photon counting spectroscopy

Figure 3 shows steady state emission spectra obtained through the excitation of extracted DOM at 405 nm and observation of fluorescence emission between 430 and 700 nm. Steady state emission spectra for all DOM extracts showed a broad band with a maxima around 471nm ± 10nm. In DOM extracts from uncharred samples (EC25 and SG25) the spectra had an additional, less pronounced band with an emission maxima around 660 nm. The band around 660 nm was consistent with the presence of pigment-like DOM while that with emission maxima around 471 nm was consistent with the humic-like DOM.[47] However, the broad nature of the band was reflective of a heterogeneous mixture of multiple fluorescent components.[39] Broad peak maxima increased with increasing pyrolysis temperature in both materials and followed the order: EC400 > SG400> EC300 > SG300 > SG0 > EC0, however emission spectra showed opposite directional shifts with temperature. Directional shifts in emission spectra are indicative of lignin-derived organic chromophore re-configurations (coumarin, flavinoids, vanillin)[39] such as molecular weight and aromaticity.[48] In Eastern Cedar, a 20 nm blue-shift occurred upon pyrolysis (481 nm in EC0 to 461 nm in EC400) and in Switchgrass, peak was red-shifted by 10nm (468 nm in SG0 to 478 nm in SG400). Possible causes of the blue-shift observed in

emission spectra of Eastern Cedar include structural changes such as a decrease in the number of aromatic rings, reduction of conjugated bonds in a chain structure, or conversion of a linear ring system to a non-linear ring; and functional group changes such as loss of carbonyl, hydroxyl and amine groups.[49] Thus Eastern Cedar and Switchgrass extracts exhibit opposing structural and functional group characteristics with increasing pyrolysis temperature.

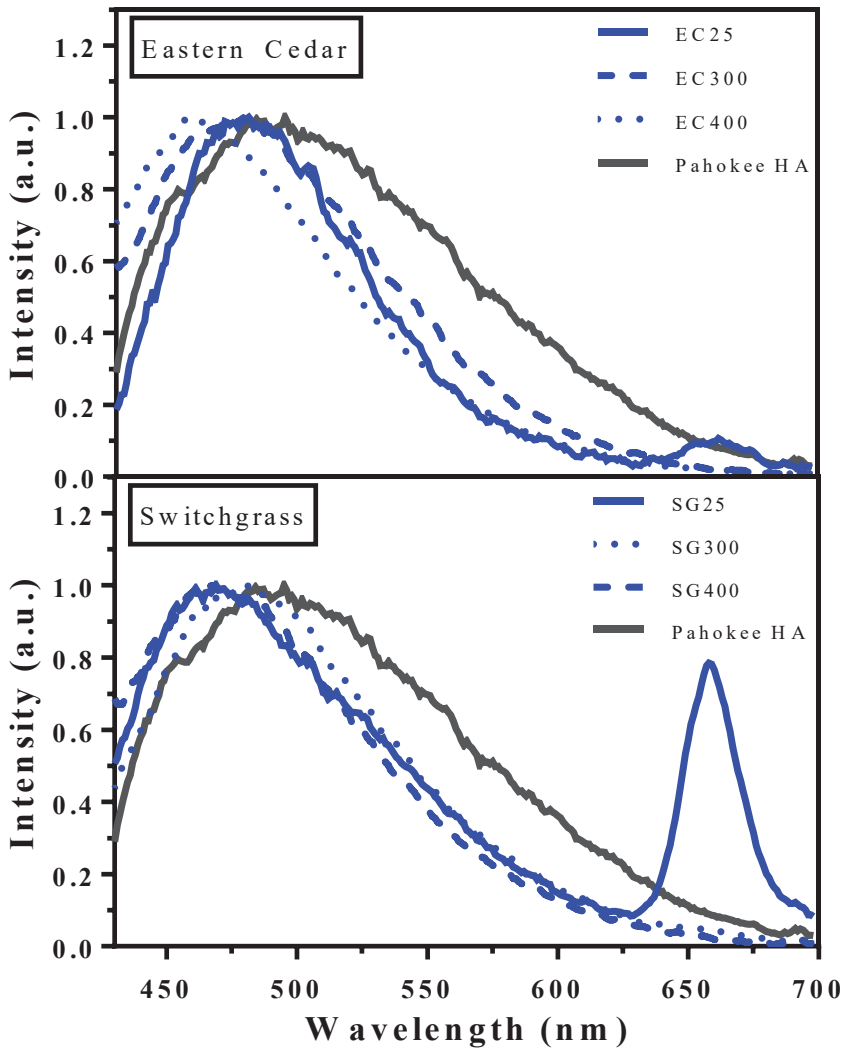

Figure 3. Normalized steady state emission spectra of DOM extracted from Eastern Cedar and Switchgrass under different heat treatment temperatures; and Pahokee peat HA. All samples were excited at λ 405 nm.

Excitation and observation wavelengths for time-resolved fluorescence decay curves were 405 and 500 nm respectively. The 405 nm laser was chosen for its significantly higher energy output than other in house lasers, thus promising the best spectra. Time-resolved fluorescence decays were tail-fitted using a multi-exponential function, with three average amplitude lifetime components within the ranges of 0.3-0.7(τ_1) ns, 1-3 ns (τ_2) and 5-8 ns (τ_3) (Table 1). Component lifetimes and percent contribution to amplitude average lifetime of unpyrolyzed material were like that of commercial Pahokee peat humic acid. Jimenez-Morais et al.[39] observed similar lifetimes in DOM from riverine and marine sources excited at 337nm. Notably, in a later study using TCSPC, Boyle et al.[40] observed three lifetime components in marine DOM and commercial HS ranging from 0-0.15 ns, 0.3-1.3 ns and 2.0-5.5 ns. Longer lifetimes observed in this study may be attributable to the more acidic environment of the fluorophore (ph ≈ 5) as opposed to neutral conditions employed by Boyle et al. HS are particularly sensitive to pH changes due to intra/inter-molecular interactions of fluorophore[50] thus influencing formation of aggregates and lengthening fluorescence. Despite the shorter lifetimes, proportions of commercial HS lifetime components at λ_{ex} 400 nm/λ_{obs} 500 nm agreed well with those observed for unpyrolyzed material in this study. Slightly longer average and component lifetimes (representing a fraction of amplitude weighted lifetime) were observed in grass vs. wood material. In both materials, the shortest lifetime component represented the largest proportion of fluorophores (α_1 = 60%) with mid and high lifetime components representing 30% (α_2) and 10% (α_3) respectively. Similarly, at λ_{ex} 400nm/λ_{obs} 500nm, Boyle et al.[40] identified lifetime proportions in Suwanee River Humic Acid and Suwanee River Fulvic Acid, of ≈ 65%, 25% and 10% for short, mid and long lifetime components respectively.

Table 1. Fluorescence lifetime values for DOM extracted from Eastern Cedar and Switchgrass under different heat treatment temperatures and Pahokee peat humic acid. All samples were excited at λ 405 nm and observed at λ 500 nm.

Materials	Parameters							
Eastern cedar	$\tau_{avg.}$ *(ns)*	τ_1*(ns)*	α_1	τ_2*(ns)*	α_2	τ_3*(ns)*	α_3	χ^2
EC25	1.1	0.36±0.02	0.61±0.04	1.46±0.05	0.31±0.01	4.50±0.12	0.09±0.00	0.697
EC300	2.8	0.64±0.05	0.41±0.03	2.72±0.06	0.41±0.01	7.96±0.10	0.18±0.00	0.992
EC400	3.1	0.67±0.06	0.36±0.03	2.81±0.06	0.45±0.01	8.10±0.10	0.19±0.00	0.965
Switchgrass								
SG25	1.5	0.42±0.03	0.58±0.03	2.63±0.06	0.32±0.01	6.36±0.14	0.10±0.00	0.880
SG300	2.8	0.69±0.05	0.55±0.02	1.60±0.05	0.35±0.01	8.07±0.10	0.10±0.00	0.964
SG400	2.7	0.68±0.05	0.43±0.03	4.38±0.05	0.42±0.01	8.42±0.11	0.15±0.00	0.984
Pahokee HA	1.2	0.34±0.02	0.62±0.03	1.60±0.04	0.30±0.01	5.62±0.10	0.08	0.981

Average and component lifetimes increased with increasing pyrolysis temperature in both materials (Fig. 4 and 5). Upon pyrolysis, average lifetimes doubled in both wood and grass material, however minimal increase was observed in 400 ºC relative to 300 ºC *Py*-DOM. In wood material at 300 ºC, α_1 decreased to 41%, with a concomitant increase to 41% and 18% observed in α_2 and α_3 respectively (Fig. 6). Although component lifetimes increased in grass material at 300 ºC, proportion of components remained relatively stable with minimal change in low and mid lifetime components (± 3%) and no change seen in high lifetime component. At 400 ºC, α_1 decreased to 36% while α_2 increased to 45%. In grass material, proportions of α_1 decreased by 12% while α_2 and α_3 increased by 7% and 5% respectively.

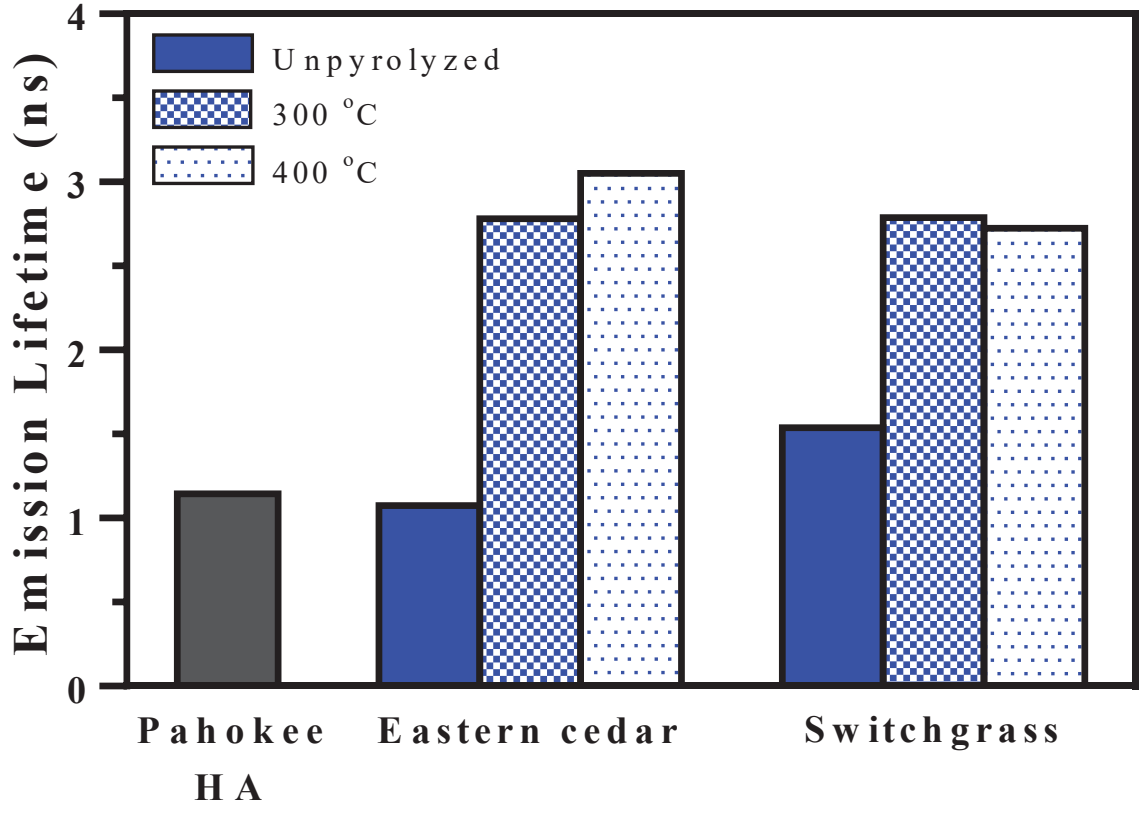

Figure 4. Average amplitude weighted lifetime of Eastern Cedar and Switchgrass DOM extracted under different heat treatment temperatures; and Pahokee peat HA.

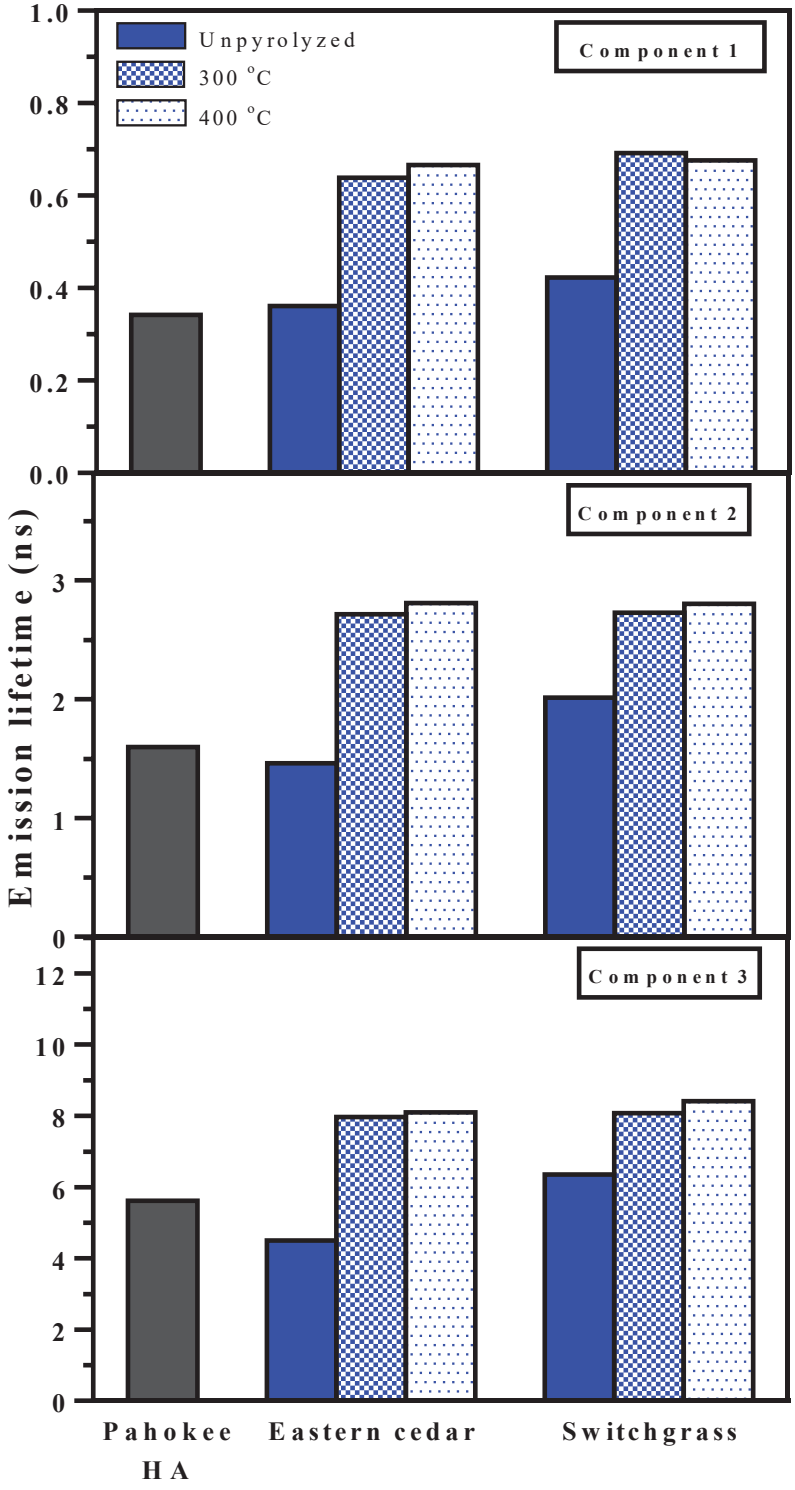

Figure 5. Amplitude weighted component lifetime (τ) of DOM extracted from Eastern Cedar and Switchgrass under different heat treatment conditions; and Pahokee peat HA.

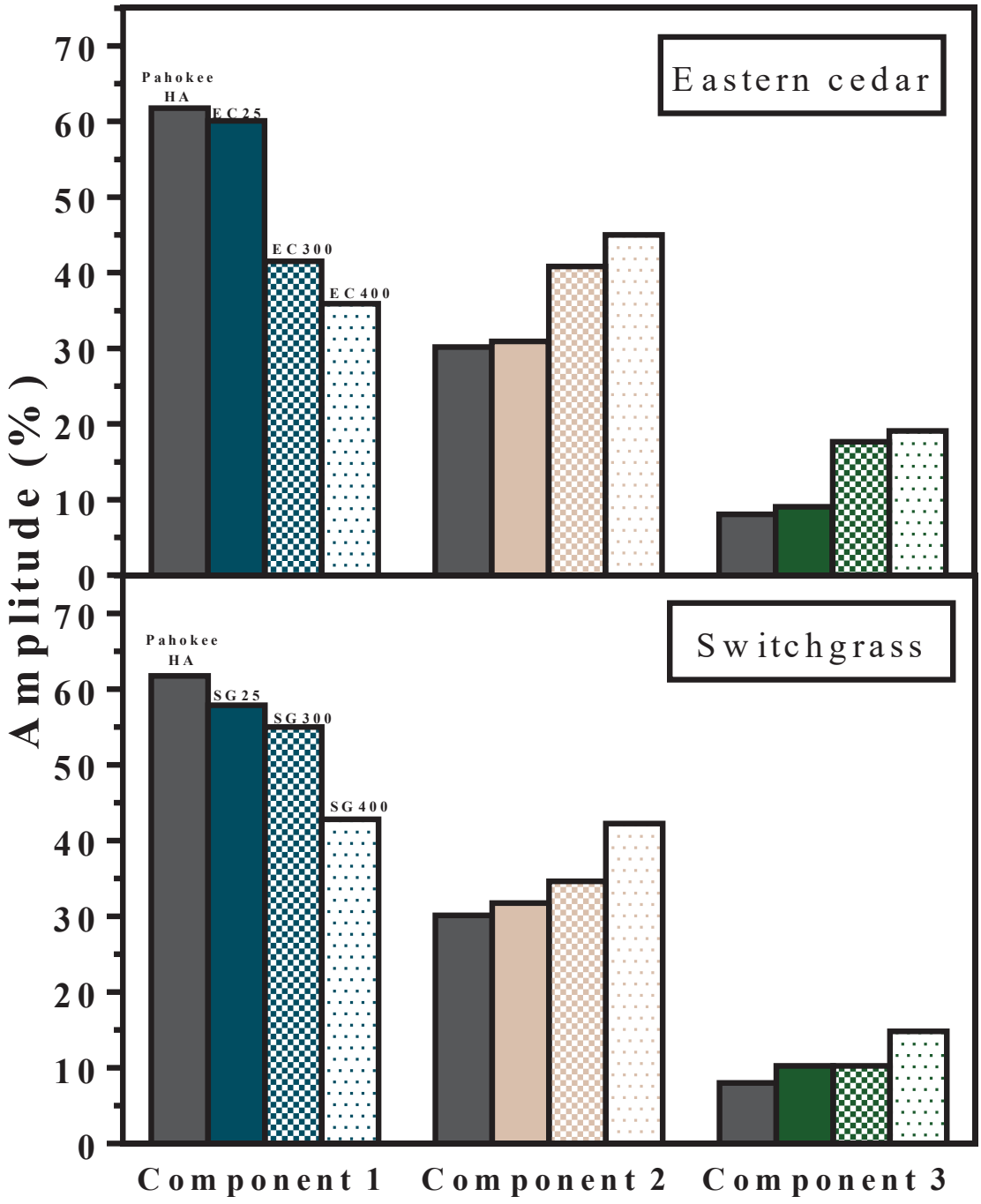

Figure 6. Amplitude weighted component proportions of DOM extracted from Eastern Cedar and Switchgrass under different heat treatment conditions and Pahokee peat HA.

The increase in average amplitude weighted lifetimes with pyrolysis is consistent with the breakdown of lignocellulose. The most common lignocellulose degradation pathways include demethylation, side-chain oxidation, and aromatic ring opening ($+O_2$)[51] hence the greater average lifetime observed in lignin-rich wood versus grass at 400 ºC. A lower proportion of lignin compounds in grass material may also explain the minimal change observed between 300 ºC and 400 ºC in grass material. Levoglucosan, a by-product of cellulose pyrolysis, may also increase fluorescence to a lesser extent. Also, formation of fluorescence decreasing carbonyl and carboxyl groups are characteristic of cellulose pyrolysis,[52] therefore a greater proportion of these compounds may be present in grass material pyrolyzed at 400 ºC. Lignocellulose degradation also explains the decrease in lower lifetime (τ_1) population and increase in mid (τ_2) and high lifetime (τ_3) population. As long chain polymers and aromatic compounds are cleaved, formation of oxygenated substituents and monomeric phenols may be driving the increase in the proportion of mid (τ_2) and high (τ_3) lifetime components.

Insights from Fourier transform ion cyclotron resonance mass spectrometry (FT-ICR MS)

Figure 7 shows an example of distribution based method of analyzing FT-ICR MS spectra. Deconvolution of C#, H/C, O/C and MW distributions provided mean (± SD) component values and proportion of signal corresponding to the mean (Table 2). C# distribution was composed of two component peaks whereas H/C and O/C ratio were composed of three component peaks. Three to five peaks were identified in MW distributions. As previously mentioned, only component peaks representing more than 10% of the signal were plotted in this study. Van Krevelen plots for unpyrolyzed and pyrolyzed grass- and wood-derived DOM, compiled from the mean H/C and O/C ratios of deconvoluted curve are shown in Figure 8 and 9. The uncharred Eastern Cedar (EC25) DOM had two distinct H/C components around 1.2 (± 0.3) and 1.8 (± 0.1); and two distinct O/C components around 0.20 (± 0.06) and 0.5 (± 0.07). Similar

H/C (1.1 ± 0.1; 1.6 ± 0.2) and O/C (0.20 ± 0.05; 0.6 ± 0.08) components were observed in the DOM from the uncharred Switchgrass (SG25) but there was an additional H/C and an O/C component centered at 1.0 ± 0.1 and 0.40 ± 0.07 respectively, that was present in SG25 but not EC25. In Eastern Cedar, H/C and O/C ratio components represented 9 and 91% of total signal respectively, whereas in grass material, 100% of signal was represented for both ratios.

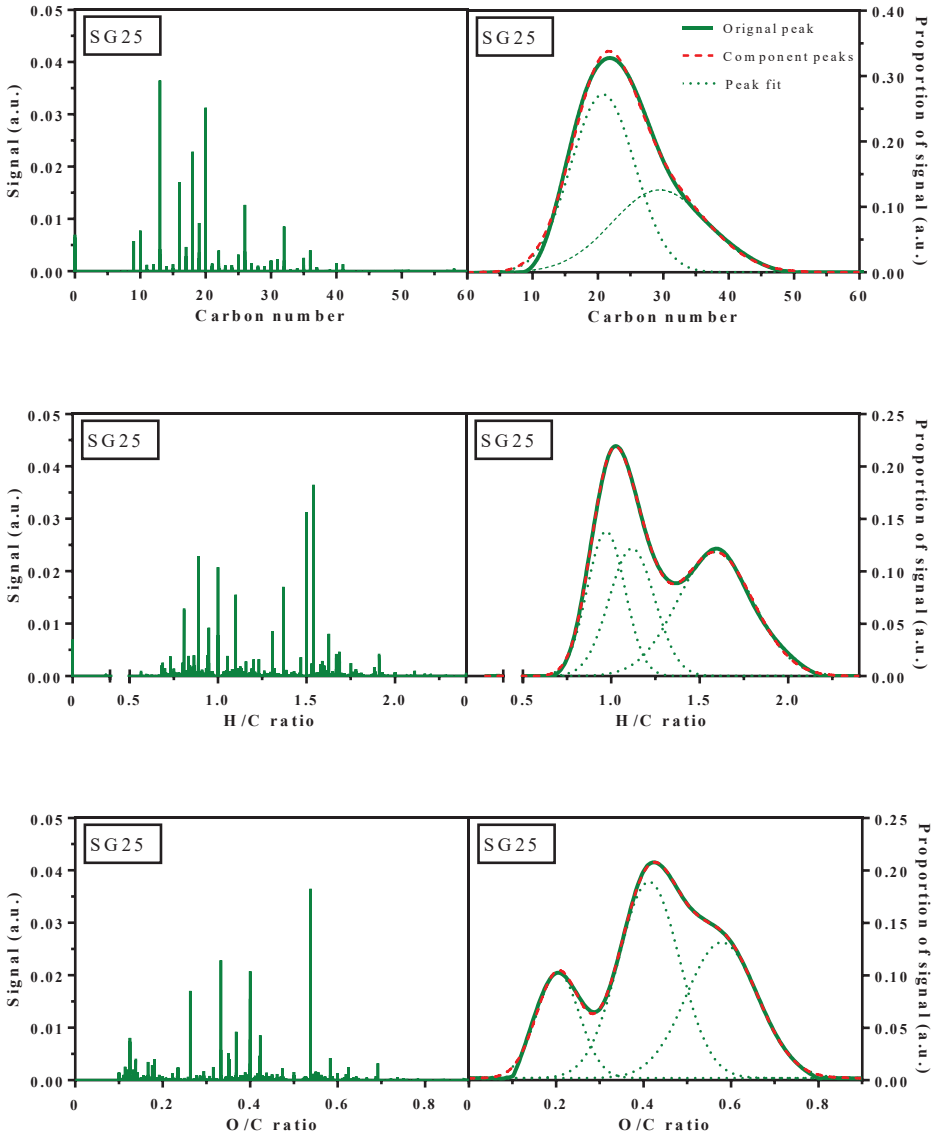

Figure 7. Binned FT-ICR MS spectra and distribution curve of Carbon number (C#), atomic H/C ratio (H/C) and atomic O/C ratio (O/C) for unpyrolyzed Switchgrass (SG25).

Table 2. Component peak centers and area of carbon number (C#), atomic H/C ratio (H/C), atomic O/C ratio (O/C), and molecular weight (MW) obtained from FT-ICR MS distribution curves.

Component peaks	EC25		EC300		EC400		SG25		SG300		SG400	
Carbon	Center	Area	Center	Area	Peak	Area	Center	Area	Center	Area	Peak	Area
1	24±5.5	0.77	19±4.0	0.45	18±3.7	0.53	21±4.9	0.59	19±3.9	0.42	18±3.6	0.54
2	36±3.4	0.23	26±7.1	55	27±7.1	0.47	29±7.2	0.41	26±6.5	0.58	27±5.6	0.46
H/C												
1	0.6±0.14	0.09	1.0±0.13	0.55	0.6±0.11	0.24	1.0±0.17	0.26	0.7±0.12	0.08	0.6±0.11	0.38
2	1.2±0.27	0.71	1.2±0.25	0.34	0.8±0.17	0.54	1.1±0.13	0.28	1.0±0.17	0.74	0.8±0.16	0.40
3	1.8±0.13	0.21	1.8±0.17	0.11	1.2±0.25	0.23	1.6±0.21	0.46	1.4±0.18	0.19	1.1±0.26	0.22
O/C												
1	0.21±0.06	0.35	0.40±0.09	0.32	0.20±0.05	0.03	0.20±0.05	0.17	0.20±0.06	0.94	0.20±0.05	0.04
2	0.51±0.07	0.56	0.50±0.08	0.60	0.48±0.09	0.95	0.40±0.07	0.46	0.5±0.10	0.03	0.50±0.08	0.90
3	0.70±0.07	0.09	0.70±0.05	0.04	0.70±0.04	0.03	0.60±0.08	0.37	0.70±0.04	0.03	0.70±0.05	0.06
MW												
1	297±40	0.05	367±70	0.67	361±67	0.71	209±30	0.04	377±75	0.71	242±27	0.02
2	410±39	0.39	547±74	0.28	544±79	0.28	394±47	0.67	562±67	0.27	364±55	0.57
3	490±40	0.44	695±63	0.05	696±27	0.01	471±61	0.13	694±30	0.02	513±97	0.40
4	600±33	0.10					598±34	0.16			694±23	0.01
5	696±29	0.03										

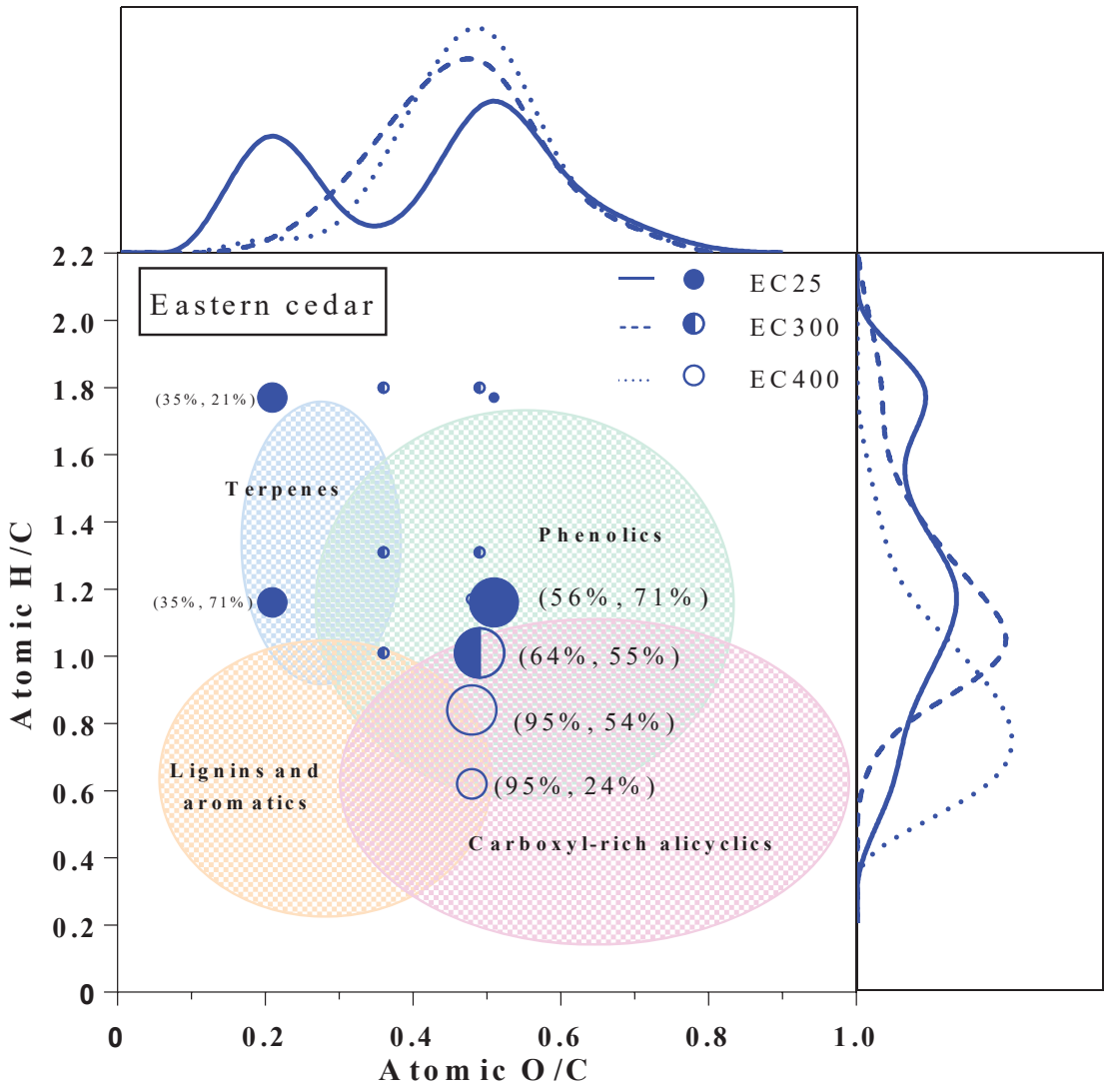

Figure 8. Van Krevelen diagram of Eastern Cedar DOM before and after pyrolysis. Points represent intersection of peak centers of deconvoluted H/C ratio (H/C) and O/C ratio (O/C) distribution curves with corresponding percent distribution. Different classes of organic matter were after Kuhnert et al.[53] and Hertkorn et al.[54]

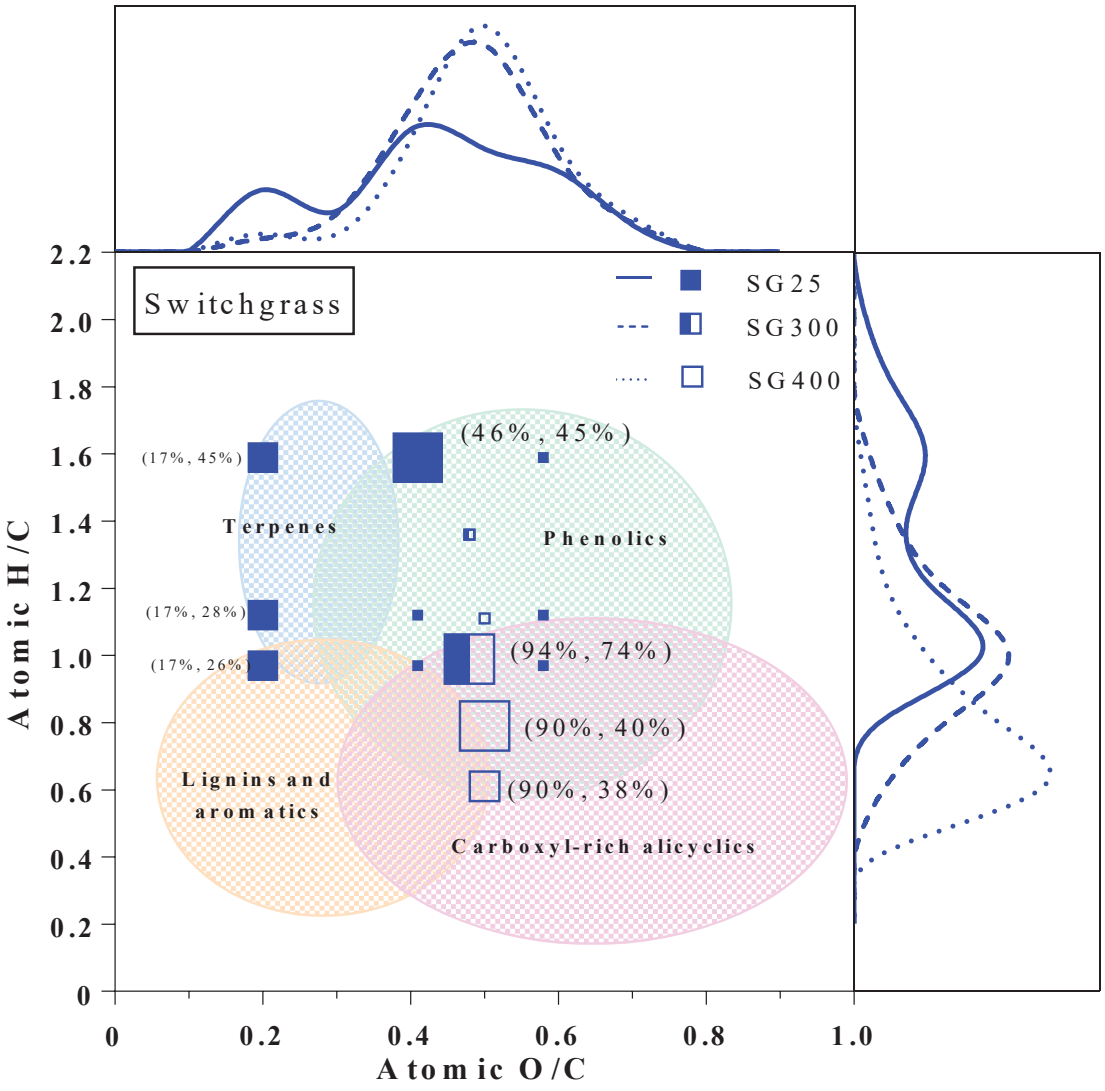

Figure 9. Van Krevelen diagram of Switchgrass DOM before and after pyrolysis. Points represent intersection of peak centers of deconvoluted H/C ratio (H/C) and O/C ratio (O/C) distribution curves with corresponding percent distribution. Different classes of organic matter were after Kuhnert et al.[53] and Hertkorn et al.[54]

The H/C and O/C ratios as well as the respective proportions observed in DOM from the unpyrolyzed EC and SG feedstocks were attributable to the hydrogen- and/or oxygen-rich aliphatic, phenolic and to a lesser extent olefinic compounds present in terrestrial DOM; derived primarily from lignocellulose biopolymers (hemicellulose, cellulose and lignin) and

terpene/terpenoids (herein referred to collectively as terpenoids) dominating plant materials.[13, 55-58] Consistent with expectations for lignocellulose-rich feedstocks,[33, 36, 59-60] phenolics accounted for the highest proportion of H/C and O/C FT-ICR MS signal in both EC25 and SG25 derived DOM (Fig. 8 and 9). The overall higher H/C ratios in DOM phenolics from SG25 (H/C = 1.6) versus that from EC25 (H/C = 1.1) is attributable to the fact that lignocellulose in grasses and other soft tissues is dominated by cinnamyl-type phenolics (cinnamyls) while that in hard tissues are dominated by syringyl-type phenolics (syringyls).[2] For example, the H/C and O/C ratios in DOM phenolics from SG25 can be replicated by assuming that the FTI-CR MS signal is being obtained from syringic acid ($[C_9H_{10}O_5]_n$) or *D*-glucose dimers or monomers covalently bonded to syringic acid via glycosidic bonds (i.e. $[O_4H_{10}C_5\mathbf{C}]_n$ **—O —**$[\mathbf{C}C_8H_9O_4]_y$). Similar glycosidic bonding between *D*-glucose subunits and cinnamyl alcohols could also account for the higher H/C and slightly lower O/C ratios in DOM phenolics in SG25, compared to that in EC25. For example, the binding of *D*-glucose units to sinapyl alcohol ($C_{11}H_{14}O_4$); (i.e. $[O_4H_{10}C_5\mathbf{C}]_n$ **—O —** $[\mathbf{C}C_{10}H_{13}O_3]_y$) yields a H/C and O/C ratio of 1.4 and 0.5 respectively.

In addition to phenolics, terpenoids were also significant components of DOM extracted from the uncharred EC and SG feedstocks (Fig. 8 and 9). Compared to phenols, these terpenoids had a lower O/C (~ 0.2 in both EC25 and SG25) with the higher relative proportions in EC25 (35%) versus SG25 (17%) being consistent with a higher terpenoid content expected in conifer versus non-conifer feedstocks.[61] The O/C signatures for terpenoids were all but absent from DOM extracted from EC and SG charcoals, produced at 300 or 400 ºC. This was indicative of the pyrolysis process thermally altering the terpenoids through, 1) condensation into non-dissolvable organic matter, 2) volatilization/mineralization to the gas phase, or 3) fragmentation and oxidation of larger molecules. The latter two possibilities are most likely in this study. Terpenoids are major contributors to the aromas plants produce and of such are expected to be

volatile upon pyrolysis. For example, α-pinene, a common terpenoid in conifers like Eastern Cedar has a boiling point of 155 ^{o}C[62] and therefore would have been easily volatilized during pyrolysis. The high degree of unsaturation – and commensurate lack of condensed domains - in the chemical structure of terpenoids also make them particularly susceptible to cleavage during the charring process.[63-64] Cleavage and fragmentation, via demethylation (the loss of CH_3) and C-C chain or alicyclic ring breaking mechanisms of organic molecules in plant materials, are well established as dominant charring steps and would account for the loss in terpenoid signature in DOM from charred samples.[65-66] The shift towards higher O/C ratios for any remaining "terpenoid-like" features (e.g. around 0.35 in EC300; Fig. 8) in charcoal-derived DOM suggests a more oxidized structure in remnants of thermal cleavage than in DOM extracted from unpyrolyzed materials.

In contrast to terpenoids, O/C signatures for the phenolics (albeit thermally-transformed) were not significantly shifted with charring of the EC or SG feedstocks. Irrespective of the feedstock material, phenolics with O/C signatures around 0.5 dominated the DOM – accounting for 56, 64 and 95% of total O/C response in DOM extracted from EC25, EC300 and EC400; as well as 46, 94 and 90% in DOM extracted from SG25, SG300 and SG400 respectively. The general persistence of phenolics, and the increase in the relative proportion of those with O/C ratios around 0.5, was indicative of their preferential accumulation with pyrolysis. Such accumulation is congruent with the preferential loss of more thermally-labile components (e.g. terpenoids) and/or thermal alteration to yield a higher proportion of thermally-stable oxygen-rich phenolics.

Thermal alteration to yield higher proportions of more thermally-stable oxygen-rich dissolved phenolics is well supported by observed changes in H/C ratios of phenolic components with increasing charring temperature (Fig. 8 and 9). For Eastern Cedar, the average H/C ratio of

the dominant phenolic component was 1.1, 1.0 and 0.8 in the DOM extracted from EC25, EC300 and EC400, respectively. With Switchgrass, the average H/C ratios for the dominant phenolic component in DOM from SG25, SG300 and SG400 were 1.6, 1.0 and 0.8 respectively. The observed changes in H/C (-0.1 to -0.2 units) to those for O/C (<<< ± 0.1 units), with increased charring temperature, was reflective of net dehydrogenation (and hence net oxidation) of phenolic components in the extracted DOM. It is also worth noting that although DOM from EC300 and SG300 showed some evidence of other phenolic components with high average H/C ratio (H/C > 1.1; Fig. 8), EC400 and SG400 lacked these components; indicating an overall intensification of net dehydrogenation between charring temperatures.

At charring temperatures ≤400 ºC, net dehydrogenation (or net oxidation) in lignocellulose is due to the sequential or simultaneous demethylation (loss of CH_3), demethenylation (loss of CH_2), demethoxylation (loss of OCH_3) and/or chemical dehydration (loss of OH and H) of hemicellulose, cellulose and lignin fractions.[65-66] The net loss of H:O (or H:C) associated with these dehydrogenation mechanisms range between 2:1 to 3:1 with varying combinations being active and needed to explain observed changes in H/C and O/C in extracted DOM from different charcoals. For example, in Figure 8, the slight loss in O/C ratio of the dominant phenolic component in EC-derived DOM points to demethoxylation and/or chemical dehydration of lignocellulose as the primary mechanisms responsible for net dehydrogenation in EC300 and EC400 DOM compared to that extracted from EC25. Conversely, the slight increase in O/C ratio (with charring temperature) for the dominant phenolic component in SG-derived DOM reflects a higher degree of preservation of structural oxygen and points to demethylation and/or demethenylation of lignocellulose side chains as the primary mechanisms driving net dehydrogenation in SG300 and SG400 DOM. The eventual loss of components with H/C ratio > 1.1 in DOM extracted from the 400 ºC charcoals is attributable to the combined intensification of

these mechanisms on the side-chains of lignin subunits and the thermally-induced ring opening/disintegration of cellulose.

Despite the similarity in hydrogen and oxygen character of wood and grass material, key differences were observable in the proportion of these components. At 300 ºC, the most dominant component of grass material accounted for 20% more of H/C ratio distribution signal and 30% more of O/C ratio distribution signal than wood material. The dominance of this component in grass relative to wood material may be attributable to the higher proportion of hemi-cellulose/cellulose in grass material. Switchgrass is composed of a higher percent of labile hemicellulosic carbohydrates (30% hemicellulose) than Eastern Cedar (19% hemicellulose)[67-68]. Hemicellulose is largely degraded at 300 ºC, however, cellulose compounds begin to degrade at 315 ºC and is mostly degraded by 400 ºC after which lignin degradation is dominant.[66] The greater thermal resistance of wood relative to grass material, as well as the lower hemicellulosic content, suggests that degradation of this labile fraction is more protected in wood material hence its presence at 300 ºC. At 400 ºC, low H/C ratio component accounted for 40-54% of signal distribution while low O/C ratio component dominated *Py*-DOM structure accounting for 90-95% of signal distribution. *Py*-DOM of Eastern Cedar and Switchgrass showed a greater loss in H/C relative to O/C and moved towards a carboxyl-rich alicyclic configuration with increasing temperature. Thermal alteration reduces H/C ratio by fragmentation and dehydration of parent material, converting *O*-alkyl C to Furan-like structures.[57, 60] Furthermore, Kramer et al.[12] also identified the presence of hydrogen deficient oxygenated structures (e.g. carboxylics) in pyrolyzed humic acids. Terpenoids have also been identified as precursors for the formation of carboxyl-rich alicyclic molecules (CRAMS).[64, 69] Hence upon pyrolysis, terpene compounds (21-71% of H/C distribution and 17-35% of O/C distribution) may drive the formation of CRAMS. Both wood and grass displayed a greater loss in H/C relative to O/C, and assumed similar

structures at 400 ºC. H/C ratios dropped from 1.2 and 1.6 in unpyrolyzed wood and grass material respectively, to 0.8 in pyrolyzed material. The dominant high H/C ratio component and the greater loss of H/C seen in grass material compared to wood material is attributable to higher proportion of carbohydrates in cellulose-rich material and lower thermal resistance.

Formulas and associated molecular weights calculated from C#, H/C and O/C ratio are presented in Table 3. Molecular weights ranged from 359 Da to 784 Da in Eastern Cedar and from 336 Da to 666 Da in Switchgrass, and were consistent with that of DOM in a forested watershed.[70] Calculated molecular weights may be slightly underestimated as nitrogen, sulfur, phosphorous and sodium distribution curves were not included in formula calculations. Formulas of calculated compounds and the two most abundant components from MW distribution curve are presented in Figure 10. The two most abundant components of MW distribution curve consisted of a dominant lower molecular weight fraction and a less dominant higher molecular weight fraction. These components represented a combined minimum of 83% (EC25) to a combined maximum of 99% (EC400) of total signal. All calculated molecular weights fell within one standard deviation of the two most abundant components from MW distribution curve except in unpyrolyzed material (50% and 73% of calculated molecular weights for EC25 and SG25 respectively).

Table 3. Calculated molecular formulas and weights for uncharred and pyrolyzed Eastern Cedar and Switchgrass material.

Sample	Molecular formula *($C_xH_yO_z$)*	Molecular weight (Da)
EC25	$C_{24}H_{28}O_5$	396
	$C_{24}H_{42}O_5$	410
	$C_{24}H2_8O_{12}$	508
	$C_{24}H_{42}O_{12}$	522
	$C_{36}H_{42}O_8$	602
	$C_{36}H_{64}O_8$	624
	$C_{36}H_{42}O_{18}$	762

Sample	Molecular formula ($C_xH_yO_z$)	Molecular weight (Da)
	$C_{36}H_{64}O_{18}$	784
EC300	$C_{19}H_{19}O_7$	359
	$C_{19}H_{25}O_7$	365
	$C1_9H_{34}O_7$	374
	$C_{19}H_{19}O_9$	391
	$C_{19}H_{25}O_9$	397
	$C_{19}H_{34}O_9$	406
	$C_{26}H_{26}O_9$	482
	$C_{26}H_{34}O_9$	490
	$C_{19}H_{47}O_9$	503
	$C_{26}H_{26}O_{13}$	546
	$C_{26}H_{34}O_{13}$	554
	$C_{19}H_{47}O_{13}$	567
EC400	$C_{18}H_{11}O_9$	371
	$C_{18}H_{15}O_9$	375
	$C_{18}H_{21}O_9$	381
	$C_{27}H_{15}O_{13}$	547
	$C_{27}H_{17}O_{13}$	549
	$C_{27}H_{32}O_{13}$	564
SG25	$C_{21}H_{20}O_4$	336
	$C_{21}H_{24}O_4$	340
	$C_{21}H_{33}O_4$	349
	$C_{21}H_{20}O_9$	416
	$C_{21}H_{24}O_9$	420
	$C_{21}H_{33}O_9$	429
	$C_{21}H_{20}O_{12}$	464
	$C_{21}H_{24}O_{12}$	468
	$C_{29}H_{28}O_6$	472
	$C_{29}H_{32}O_6$	476
	$C_{21}H_{33}O_{12}$	477
	$C_{29}H_{46}O_6$	490
	$C_{29}H_{28}O_{12}$	568
	$C_{29}H_{32}O_{12}$	572
	$C_{29}H_{46}O_{12}$	586
	$C_{29}H_{28}O_{17}$	648
	$C_{29}H_{32}O_{17}$	652
	$C_{29}H_{46}O_{17}$	666
SG300	$C_{19}H_{19}O_9$	391
	$C_{19}H_{26}O_9$	398
	$C_{26}H_{26}O_{12}$	530
	$C_{26}H_{35}O_{12}$	539

Sample	Molecular formula ($C_xH_yO_z$)	Molecular weight (Da)
SG400	$C_{18}H_{11}O_9$	371
	$C_{18}H_{14}O_9$	374
	$C_{18}H_{20}O_9$	380
	$C_{27}H_{16}O_{14}$	564
	$C_{27}H_{21}O_{14}$	569
	$C_{27}H_{30}O_{14}$	578

By combining ratio distributions and molecular weight distribution curves, the molecular formula and mass of each sample can be reasonably inferred. For example, in EC25, the two most abundant MW components, representing a combined 83% of signal distribution were 410 ± 39 Da and 490 ± 40. Additionally, the calculated molecular formula of compounds falling within one standard deviation of these components was $C_{24}H_{28\text{-}42}O_{5\text{-}12}$. Therefore, it can be inferred that compounds with a molecular formula of $C_{24}H_{28\text{-}42}O_{5\text{-}12}$ and a mass range between 371-530 Da is most representative of EC25. Likewise, in SG25, most compounds have a molecular formula and weight of $C_{21\text{-}29}H_{20\text{-}46}O_{4\text{-}12}$ and 347-633 Da respectively. In pyrolyzed material, DOM had the following molecular formulas and weights: $C_{19\text{-}26}H_{19\text{-}47}O_{7\text{-}13}$ in EC300 (297-621 Da); $C_{19\text{-}26}H_{19\text{-}35}O_{9\text{-}12}$ in SG300 (302-629 Da); $C_{18\text{-}27}H_{11\text{-}32}O_{9\text{-}13}$ in EC400 (294-623 Da) and $C_{18\text{-}27}H_{11\text{-}30}O_{9\text{-}14}$ in SG400 (309-610 Da). The dominance of oxygenated compounds ($C_xH_yO_z$) agreed well with previously published studies of DOM in terrestrial and marine aquatic systems.[11, 51]

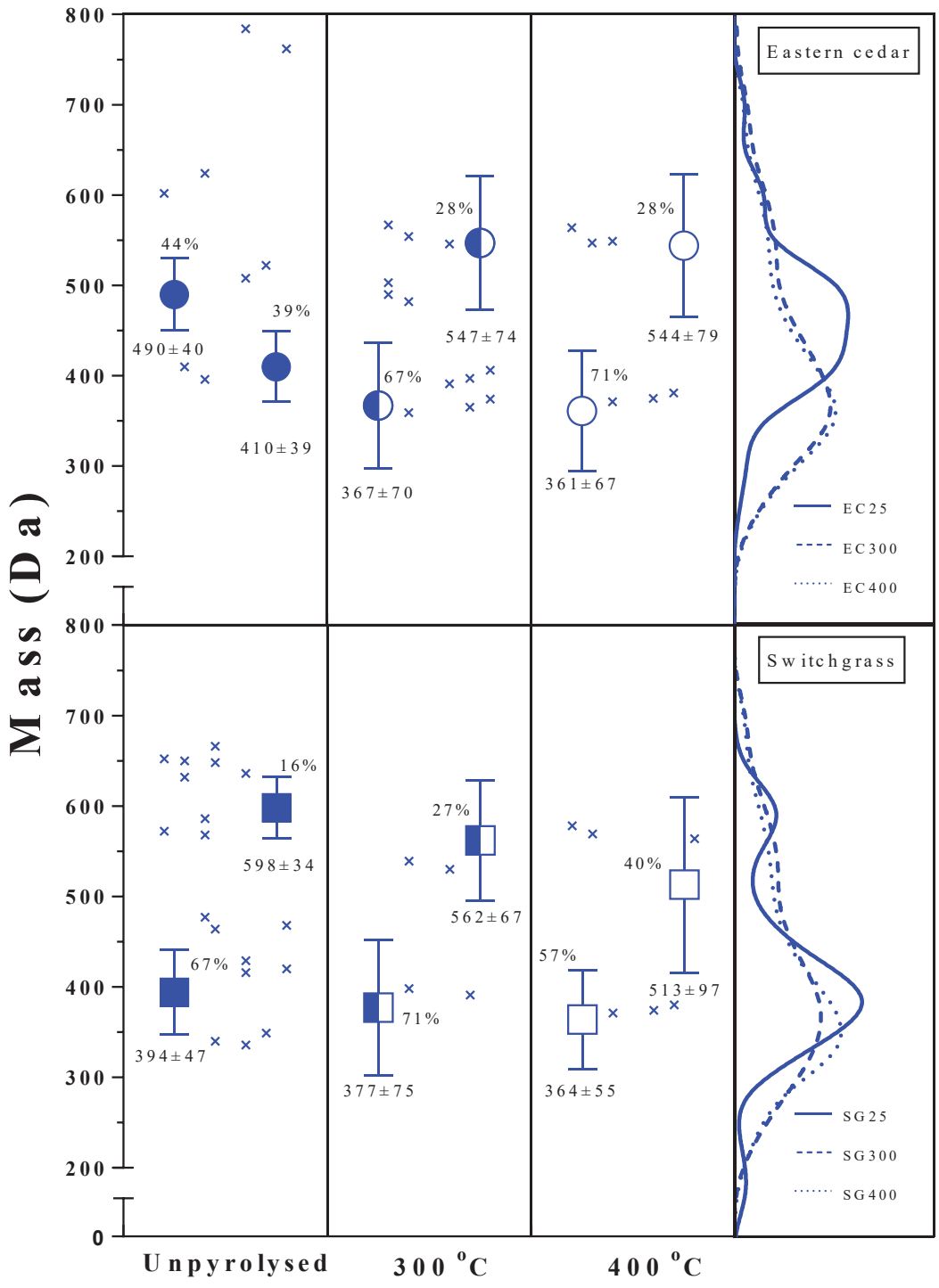

Figure 10. Two most dominant components of molecular weight distribution curve (± 1 SD) and calculated molecular weights (x) from Carbon number (C#), atomic H/C ratio (H/C) and atomic O/C ratio (O/C) for Eastern Cedar and Switchgrass.

CHAPTER II

ENERGY-DEPENDENT RESPONSE OF PYROGENIC DISSOLVED ORGANIC MATTER (*PY*-DOM) AS ELUCIDATED THROUGH STEADY STATE AND TIME RESOLVED FLUORESCENCE SPECTROSCOPY

Introduction

The reactivity and hence susceptibility to degradation of *Py*-DOM is predominantly a function of feedstock chemistry and pyrolysis conditions[71-73] with lightly charred plant materials being more susceptible than their more condensed counterparts.[74] Biotic degradation of *Py*-DOM is well understood,[75-76] however its abiotic transformation (e.g. via photodegradation) is not. The more aromatic nature of *Py*-DOM compared to non-pyrogenic DOM has been suggested as a key factor in its photodegradability with more aromatic *Py*-DOM being more photo-reactive and producing the more labile compounds favored by microbes.[22, 25] Stubbins et al.[22] reported a 95% decrease in marine *Py*-DOM after 28 days of artificial irradiation compared to 76% in DOM. However as noted in Chapter I, and other studies,[9, 11, 77-78] *Py*-DOM of wood and grass material contain a significant proportion of highly oxygenated carboxylic-rich alicyclic molecules (CRAM). In addition, photodegradation of *Py*-DOM produces highly oxidized compounds of unknown reactivity.[25] Consequently, despite improved estimates of *Py*-DOM in aquatic environments,[6, 79-82] significant knowledge gaps exist with respect to the rate and mechanistic aspects of their photodegradation.

Chapter I highlighted key differences in the components of base extracted DOM/*Py*-DOM as a function of pyrolysis and feedstock using fluorescence spectroscopy and FT-ICR MS. This Chapter identifies systematic changes in the fluorescence behavior of different *Py*-DOM (in response to solar exposure) to develop quantitative perturbation-response relationships under conditions of varying exposure duration, and solution chemistry. Both steady state and time-

resolved fluorescence spectroscopy measurements were utilized to elucidate the bulk rate of photodegradation and the underlying components contributing to its photodegradation. Specific focus will be placed, on the monitoring of changes in the operationally defined fulvic-like (soluble under all pH conditions) and humic-like (soluble only under basic pH conditions) components of *Py*-DOM extracted from a natural grass-derived and a wood-derived charcoal.

Materials and Methods

Preparation of charcoals and extraction of Py-DOM

Plant material was sampled from the Fort Worth Nature Center (Fort Worth, TX, USA) in January 2017. Material preparation prior to charring was as outlined in Chapter I (pg. 8). Samples were then tightly placed into quartz tubes; tubes were tightly wrapped in aluminum foil (to produce oxygen-limited conditions) and then charred in a laboratory tube furnace (Thermolyne, Dubuque, IA). Charring was from room temperature to the target pyrolysis temperatures of 400 °C at a ramp rate of 25-30 °C/min and kept at target pyrolysis temperature for 1 h. After the one hour pyrolysis period, the furnace was kept closed and allowed to cool to room temperature before the resulting charcoals were removed. Charcoals were then ground, sieved (250 μm) and stored in air-tight glass jars at room temperature.

Pyrolysis of feedstock produces a suite of (partially) oxidized lignocellulose products of varying solubility, thus, varying rates of photodegradation is expected among different *Py*-DOM and between DOM and *Py*-DOM.[13, 83] For example, humic substances (humic acid and fulvic acid) possess common aromatic/aliphatic structures and functional groups such as carboxyls and phenols, however, the size and configuration of these compounds vary.[32] As such, both the humic acid and fulvic acid fractions were targeted in extracting *Py*-DOM from the charcoals. DOM from feedstock and charred samples were extracted using ultra-high quality water (18MΩ; ThermoScientific, Waltham, MA) and 0.1M NaOH. Between 1 and 2 g of charcoal were

weighed into 50-mL centrifuge tubes and 40 ml of extractant added to make an unaltered feedstock/charcoal-extractant suspension. Two DOM extraction approaches were initially tested. One with unaltered feedstock/charcoal-extractant suspensions shaken on a horizontal shaker for 24 h at room temperature and another using microwave-assisted extraction (8 ºC/min to 80 ºC and held for 1.5 h). For both extractants (water and NaOH), microwave assisted yielded more DOM. As such, this technique was chosen. Following microwave-assisted extraction, samples were vacuum filtered (0.7µm glass fiber filter; Pall Corporation, NY) and the resulting DOM/*Py*-DOM-containing extract used as the stock solution for fluorescence experiments. DOM/*Py*-DOM nomenclature was referenced by parent material abbreviation, pyrolysis temperature, and extractant, thus Eastern Cedar pyrolyzed a 400 ºC and extracted using water was referenced as EC400W while that extracted using NaOH was referenced as EC400B.

Sample irradiation

Stock solution for photodegradation experiments were diluted with ultra-high quality water to 200 mL and adjusted to pH 5 using 0.1 N HCL. Photodegradation experiments were conducted in specialized quartz tubes built in house. Internal and outside diameter of quartz tubes was 21 mm and 25 mm respectively, with an internal volume of ≈ 125 ml. Light-exposed and dark control treatments (wrapped in aluminum foil) were filled with 100mL of stock solution, crimped and placed in autoclave at 121 ºC for 30 min. A 20G syringe needle was placed in septa of each tube to facilitate the release of any accumulated gases. After autoclaving, samples were placed in a dark container to cool to room temperature. A specially designed plywood box measuring 4ft x 4ft x 1ft (LXWXH) was built to hold quartz tubes exposed to sunlight. Box was placed in direct sunlight and 2 ml of sample was collected in triplicate after 1h, 2h, 4h, 6h, and 8h (Fig.11). Solar irradiance was recorded at 5 min intervals using a solar irradiance meter (Seaward, Tampa, FL) and was typical with that expected in March in the area

(16.2-18 MJ m^{-2}; Fig. 12).[84] Absorbance (UV-vis), steady state fluorescence, and fluorescence lifetime measurements were carried out concurrently with triplicate sampling.

Figure 11. Quartz tubes containing *Py*-DOM/DOM extracts of Eastern Cedar and extracts exposed to solar radiation. Solar irradiance meter (pictured in yellow) recorded at 5 minute intervals.

Absorbance, steady state fluorescence and time-resolved fluorescence measurements

All absorbance and fluorescence measurements were done at a path length of 1 cm. For absorbance, samples were measured at wavelengths of 254, 365 and 405nm prior to sunlight exposure and at each sampling interval (1h, 2h, 4h, 6h and 8h) using an Evolution 220 UV-vis spectrophotometer (ThermoScientific, Waltham, MA). The ratio of absorbance at λ_{abs} 254 nm (E2) to λ_{abs} 365 nm (E3) were used to calculate the E2:E3 indicator; a UV-vis proxy of DOM size and structure, with an increase in E2:E3 ratio indicating a decrease in molecular size and

aromaticity.[85] Steady state fluorescence emission spectra for each sample were collected at an excitation wavelength of 405 nm and observed between emission wavelengths of 430 nm and 700 nm (Cary Eclipse fluorescence spectrophotometer; Varian Inc., Palo Alto, CA). The fluorescence emission spectra for both the 0.1 M NaOH solution and water was used to correct the sample spectra for Raman scattering effects. Steady state fluorescence spectra were used to determine suitable excitation and observation parameters for the lifetime measurements. Fluorescence lifetime measurements followed the same procedure as outlined in Chapter I (pg. 10).

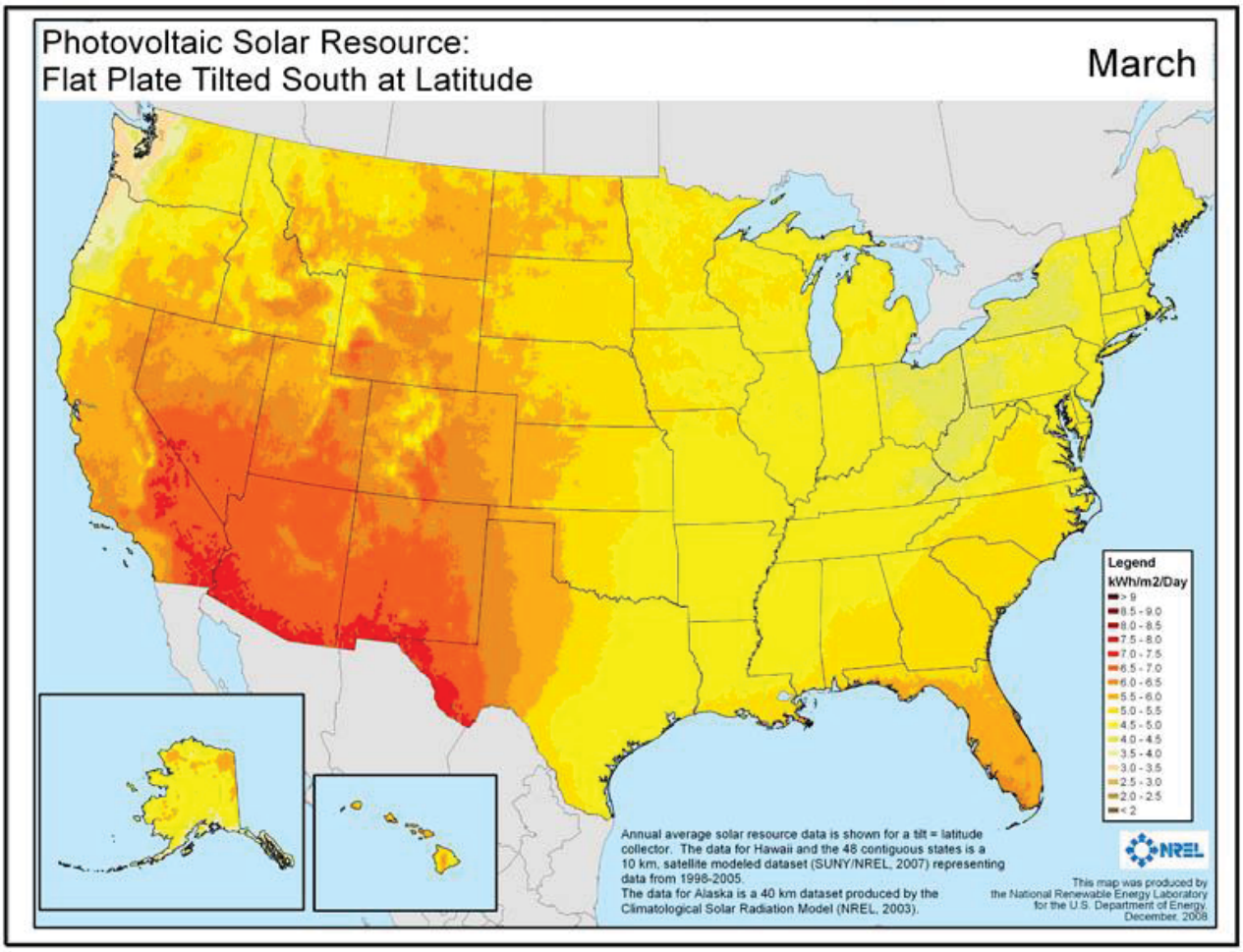

Figure 12. Average energy (kW h m^{-2} d^{-1}) in March across the conterminous United States between 1998 and 2005.[84]

Results and Discussion

Energy-induced changes to bulk characteristics of extracts

Prior to exposure, sample absorbance at 254 nm ranged from 0.347 in SG400B to 1.26 in EC25W and from 0.064 in EC400B to 0.189 in EC25W at 365 nm. Values of *E2:E3* for Eastern Cedar followed the order (EC25B (3.44) < EC400W (5.80) < EC25W (6.67) ≈ EC400B (6.83). In Switchgrass, *E2:E3* ascended in the order SG400W (2.64) < SG400B (3.61) < SG25W (4.15) < SG25B (5.39). In general, *E2:E3* was higher in base- versus water-extracted DOM, unpyrolyzed versus pyrolyzed DOM and wood versus grass DOM. The exception to this trend was seen in EC25B which had a lower *E2:E3* than EC25W, EC400B and SG25B respectively. The lower *E2:E3* may be due to the high proportion of terpene compounds present in base-extracts of Eastern Cedar identified by ultra-high resolution mass spectrometry in Chapter I. Base extracts of Eastern Cedar contain a higher proportion of humics than water extracts; in addition, terpene compounds are largely degraded by 400 ºC and would also be more prevalent in conifer versus non-conifer feedstock. Therefore, terpene compounds are expected to be more prevalent in base- versus water-extracted, pyrolyzed versus unpyrolyzed and conifer versus non-conifer feedstock DOM. It is not always explicit as to whether *E2:E3* is a better indicator of molecular size and/or aromaticity in this sample set. For example, results suggest that base-extracted DOM, pyrolyzed DOM and wood DOM generally contains smaller and/or less aromatic components than water-extracted DOM, unpyrolyzed DOM and grass DOM respectively. However, while smaller, less aromatic compounds is expected in pyrolyzed versus unpyrolyzed materials, such a trend is not expected in base- versus water-extracted and wood versus grass DOM.

Another use of the *E2:E3* proxy is in the assessment of photodegradation extent.[77] Hence *E2:E3* values at each sampling interval can be used to estimate the relative size/aromaticity of

materials with increasing solar exposure. Figure 13 shows irradiance curve plotted from integration of energy measurements taken at 5 min. intervals. Total energy input after 1h, 2h, 4h, 6h and 8h was 1.3, 3.4, 9.1, 15.1 and 19.2 MJ m^{-2} respectively (Table 4). Except for EC25W, *E2:E3* increased with increasing sunlight exposure consistent with an increase in the proportion of smaller and/or less aromatic components and pointing to evidence for photodegradation via the preferential breakdown of large, aromatic structures (Fig. 14). In EC25W, *E2:E3* increased after 1 h but decreased thereafter. While this does not exclude photodegradation in EC25W, it suggests a different mechanism than in other extracts.

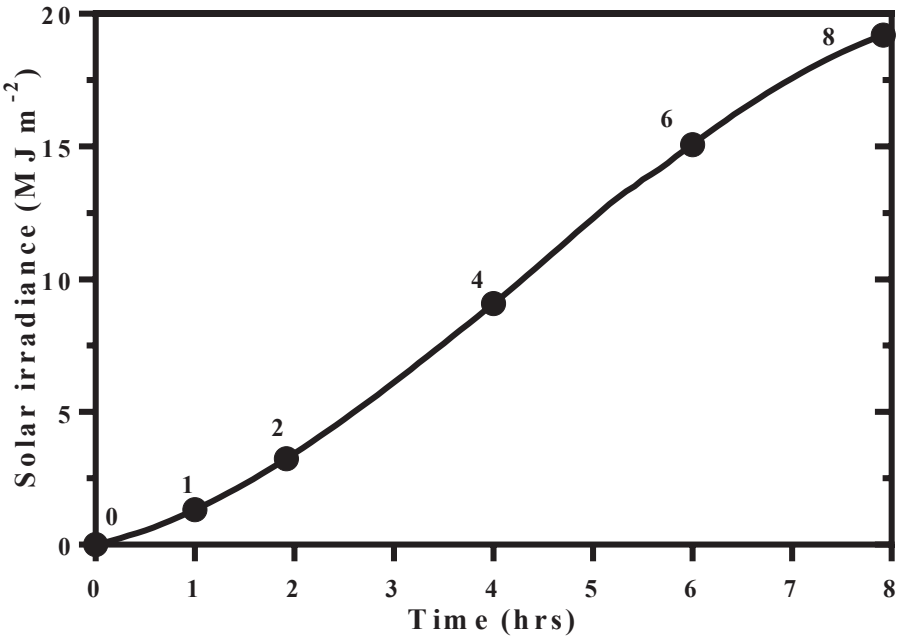

Figure 13. Integrated irradiance measurements taken at 5min interval. Labelled points on curve indicate sampling times.

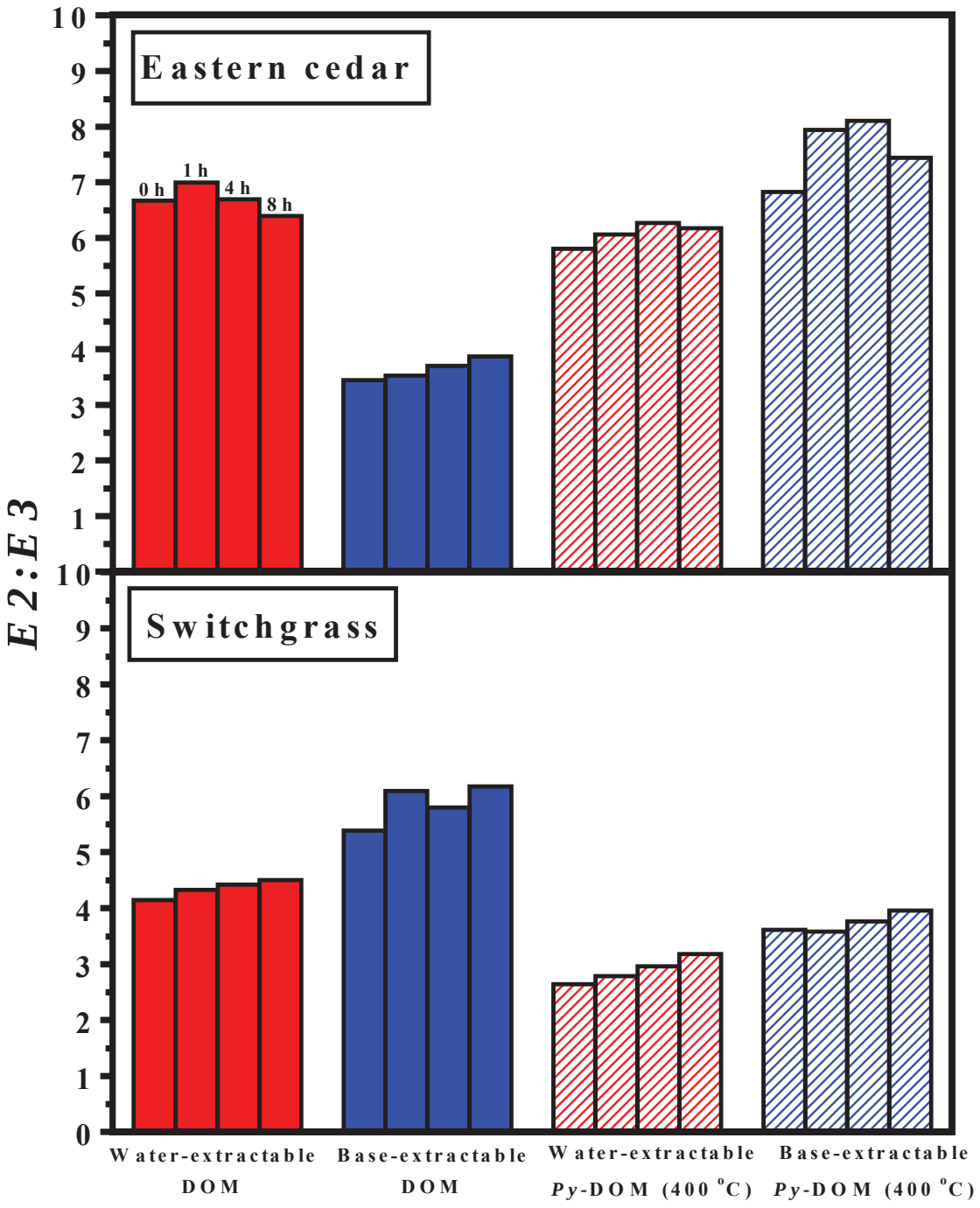

Figure 14. *E2:E3* of Eastern Cedar and Switchgrass extracts at select sample intervals (0h, 1h, 4 h and 8h).

Table 4. Sampling times and corresponding incident energy during that period.

Time (hours)	Energy input (MJ m^{-2})
0	0
1	1.32
2	3.44
4	9.09
6	15.1
8	19.2

Steady state emission spectra (λ_{ex} 405 nm) collected at each sampling interval and revealed a broad peak centered around 440 nm – 470 nm in all samples, consistent with that expected of a heterogeneous mixture of multiple fluorescent components.[39] A second peak, centered at 520 nm was observed only in EC25B and was not seen in spectra after 1 h of exposure. Given the small change in *E2:E3* ratio over the same period, (Fig. 14), it is unlikely that the loss of this second peak is associated with any drastic shifts in molecular size/aromaticity of DOM. For quantitative spectral comparison, temporal fluorescence intensity (I) of each sample (0h, 1h, 2h, 4h, 6h, 8h) was divided by the initial fluorescence intensity (I_0) and presented as I/I_0. In all samples, I/I_0 decreased after 8 hours of exposure and was fitted using a non-linear regression one phase decay model or an initial plateau constrained one phase decay model (for EC25B) represented by:

$$(1) \quad \frac{I}{I_0} = \frac{1-\beta}{e^{\phi x}} + \beta$$

or

$$(2) \quad \frac{I}{I_0} = \frac{1-\beta}{e^{\phi (x-x_0)}} + \beta$$

where x_0 is the time at which the decay begins, β is the y value at infinite times, and ϕ is the pseudo-first order rate constant of the reaction. Other parameters derived from the model include

the *half-life* ($t_{1/2}$) of the reaction, and the degraded fraction (DOM_{deg}) computed as *1 – residual*, where *residual* refers to remaining DOM after 8 hours of exposure.

Model fit parameters for all samples are presented in Table 5. Pyrolysis and extractant had no effect on DOM_{deg} however DOM from EC samples were more photodegraded than that from Switchgrass after 8 hours of sunlight exposure (Fig. 15). Switchgrass samples, lost roughly 49 to 55% of DOM after 19.2 MJ m^{-2} of energy input over 8 h compared to EC samples which lost 72 to 85% for the same energy input over the same period. The greatest loss was observed in EC25W. This was surprising because the *E2:E3* ratio of EC25W decreased only slightly after 19.2 MJ m^{-2}, suggesting a slight increase in molecular size/aromaticity. However, as previously mentioned, *E2:E3* of EC25W increased after 1.3 MJ m^{-2} energy input. This decrease in size/aromaticity after 1 h agrees well with the comparatively short $t_{1/2}$ (0.45 h) and high ϕ (1.55 h^{-1}) which suggest that a large fraction of EC25W was degraded within 1 h (1.3 MJ m^{-2}).

Table 5. Photodegradation model fit parameters for Eastern Cedar and Switchgrass. DOM_{deg} calculated as 1-*resiudal* where *residual* refers to the remaining DOM after 8 hours.
$t_{1/2} = \frac{ln(2)}{\phi}$

Materials	Parameters			
Eastern Cedar	DOM_{deg}	$t_{1/2}$ *(h)*	*Rate* ϕ (h^{-1})	R^2
EC25W	0.85(±0.01)	0.45	1.55(±0.12)	0.998
EC400W	0.72(±0.03)	1.51	0.46(±0.06)	0.994
EC25B	0.75(±0.03)	1.05	0.66(±0.13)	0.998
EC400B	0.72(±0.02)	1.39	0.50(±0.05)	0.997
Switchgrass				
SG25W	0.52(±0.00)	0.71	0.98(±0.04)	0.998
SG400W	0.51(±0.06)	1.21	0.57(±0.20)	0.949
SG25B	0.49(±0.02)	0.43	1.61(±0.36)	0.984
SG400B	0.55(±0.13)	0.96	0.72(±0.13)	0.983

Values of ϕ were inversely related to $t_{1/2}$ such that water-extracted pyrolyzed Eastern Cedar had the lowest ϕ (0.46 ± 0.06) and longest $t_{1/2}$ (1.51) while base-extracted unpyrolyzed Switchgrass had the highest ϕ (1.61 ± 0.36) and shortest $t_{1/2}$ (0.43). It should be noted however, that standard error of ϕ for pyrolyzed material indicated no significant difference between EC400W and SG400W as well as EC400B and SG400B. All half-lives except EC25B were less than 2 h thereby suggesting that less than 3.44 MJ m^{-2} of energy was required to degrade 50% of initial DOM. Switchgrass samples had a higher ϕ and shorter $t_{1/2}$ than Eastern Cedar samples in similar treatments except in unpyrolyzed water extracts. These results suggest that although DOM_{deg} was higher in wood than in grass, the structure and composition of grass extracts degrade more readily than wood material. Unpyrolyzed material showed a higher susceptibility to photodegradation than pyrolyzed samples, having both a higher ϕ and shorter $t_{1/2}$, however standard error indicated no statistical difference between ϕ of EC25B (0.66 ± 0.13) and EC400B (0.50 ± 0.05). Extractant had minimal effect on the photodegradability of DOM in pyrolyzed extracts, however in unpyrolyzed samples, the opposite is true. EC25B had a higher ϕ and shorter $t_{1/2}$ than EC25W, however, in grass material, SG25W had a lower ϕ and longer $t_{1/2}$ than SG25B.

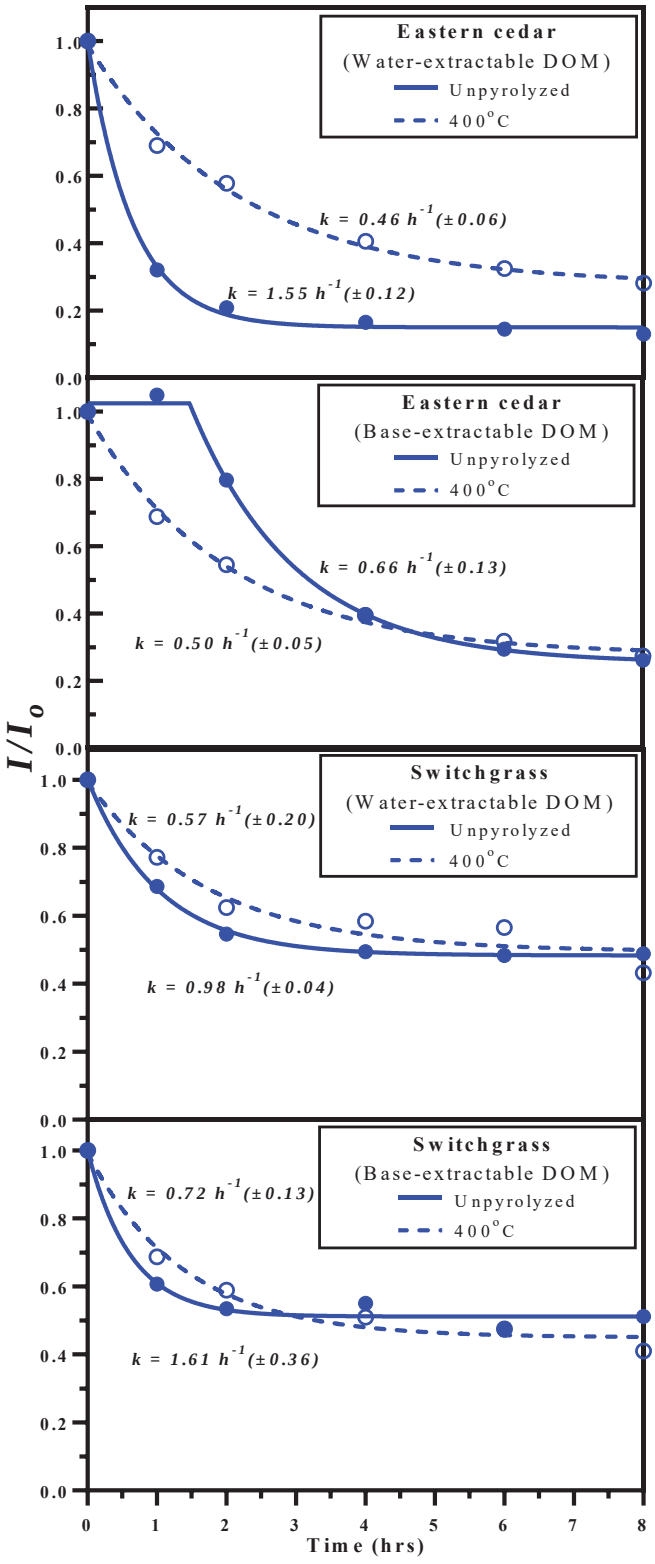

Figure 15. Non-linear regression curve fit of *I/I0* for Eastern Cedar and Switchgrass over an 8-hour period of sunlight exposure.

Energy-induced component specific response

Time-resolved fluorescence measurements were performed under standard conditions as described previously with an excitation wavelength at λ_{ex} 405 nm and the emission was monitored at λ_{obs} 500 nm. Amplitude average lifetimes were 1.4 (EC25B), 2.4 (EC25W), 4.1 (EC400B) and 4.5 ns (EC400W) for DOM extracted from Eastern Cedar and 1.7 (SG25B), 2.3 (SG25W), 2.9 (SG400B), and 3.2 ns (SG400W) for that extracted from Switchgrass (Table 6). In general, amplitude average lifetimes were longer in pyrolyzed material, water extracted DOM, and wood feedstock (except in EC25B) than in unpyrolyzed material, base-extracted DOM and grass feedstock respectively. Deconvolution of multi-exponential fluorescence decay curve revealed three components with amplitude weighted lifetimes of: 0.4-1.2 ns (τ_1), 2-5 ns (τ_2) and 5-11 ns (τ_3). Each component followed a similar trend with regards to extractant, material and pyrolysis as seen in amplitude average lifetimes (i.e., lifetimes were longer in pyrolyzed material, water extracted DOM, and wood feedstock for each component). The proportion of fluorophores contributing to the total amplitude weighted fluorescence followed the order $\alpha_1 > \alpha_2 > \alpha_3$ except in EC25W and EC400W extracts which followed the order $\alpha_2 > \alpha_1 > \alpha_3$.

After 8 hours of exposure, both τ_1 and τ_2 decreased, whereas τ_3 generally increased in all samples except EC25B (Fig. 16, 17 and 18). In general, percent change in α was higher in unpyrolyzed samples than in pyrolyzed samples indicating that fluorophores in DOM from unpyrolyzed materials were more responsive to solar inputs than DOM from pyrolyzed materials (Fig. 19, 20, 21 and 22). For example, in EC25W, 19 MJ m^{-2} of energy input decreased α_2 and α_3 by 56% and 28% respectively, however, in EC400W, the same energy input decreased α_2 and α_3 by only 10% and 4% respectively. Photodegradation of components in Eastern Cedar material was also influenced by extractant. Both α_2 and α_3 were photodegraded in EC25W and EC25B, however, energy required to degrade α_3 was higher in base than in water extracts. In EC25W,

24% of α_3 was lost after 1.3 MJ m^{-2} energy input, however, in EC25B, no loss was observed below 9.1 MJ m^{-2} and only 8% was lost after 19.2 MJ m^{-2}.

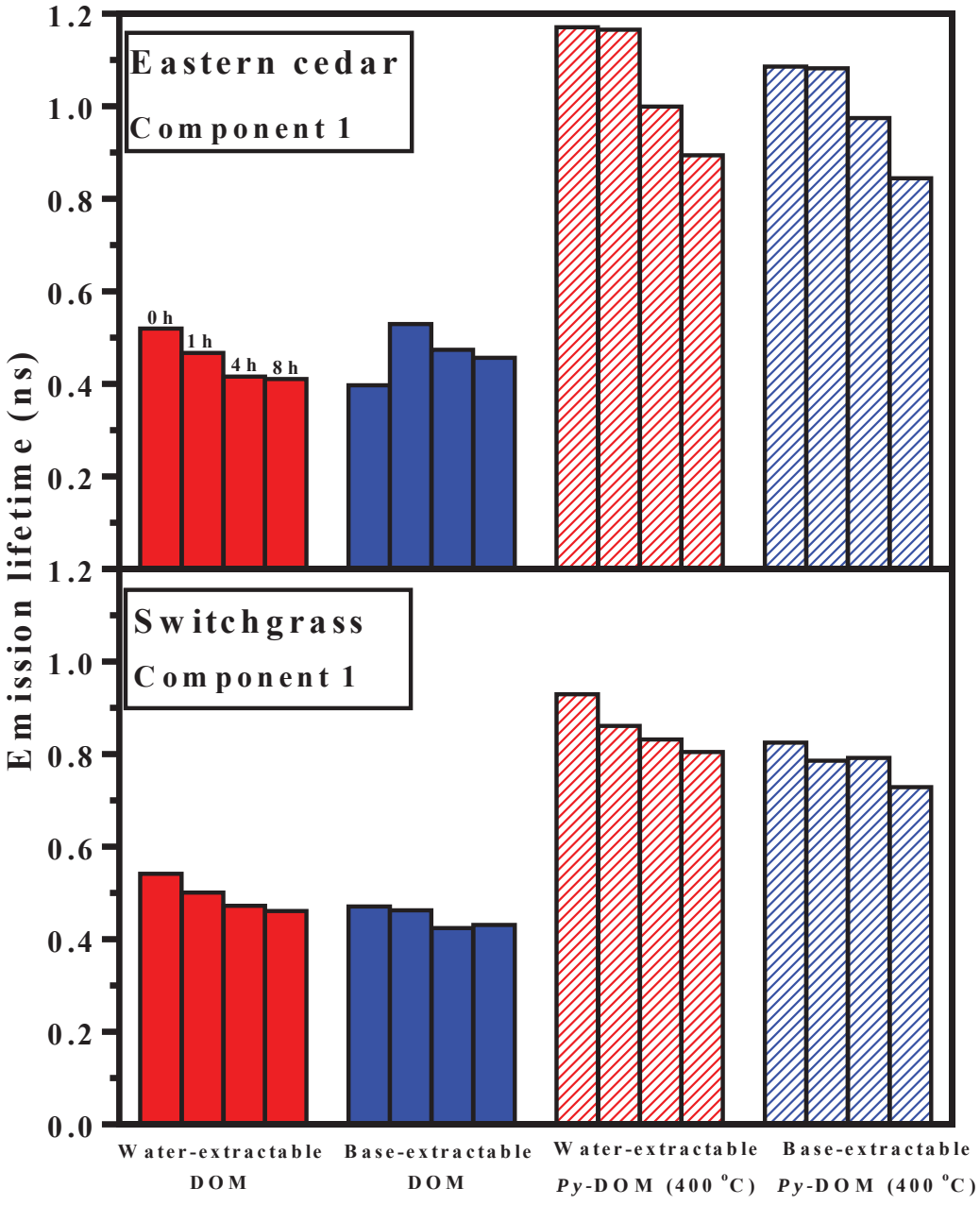

Figure 16. Component 1 lifetimes for Eastern Cedar and Switchgrass at sampling intervals of 0h, 1h, 4h, and 8h.

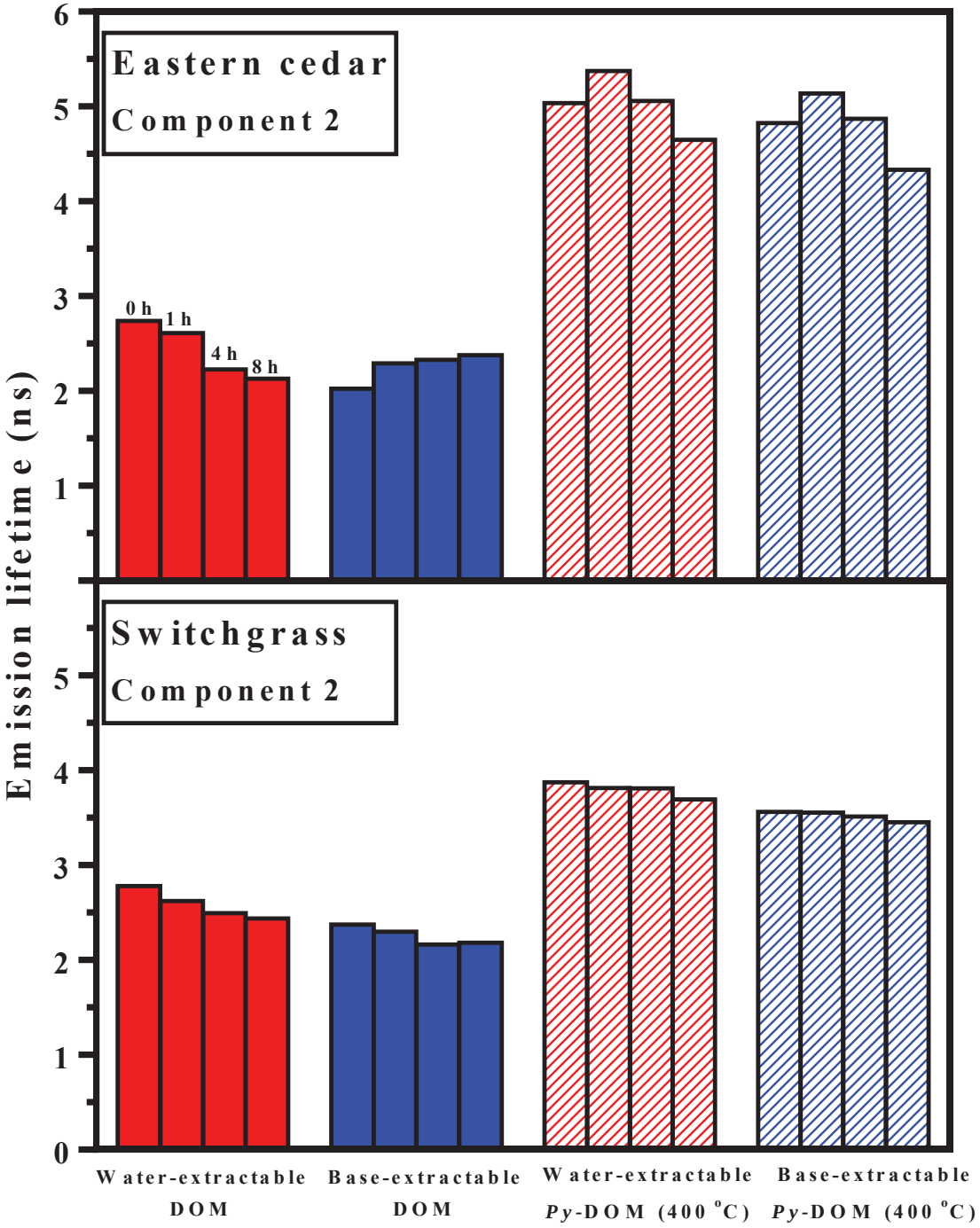

Figure 17. Component 2 lifetimes for Eastern Cedar and Switchgrass at sampling intervals of 0h, 1h, 4h, and 8h.

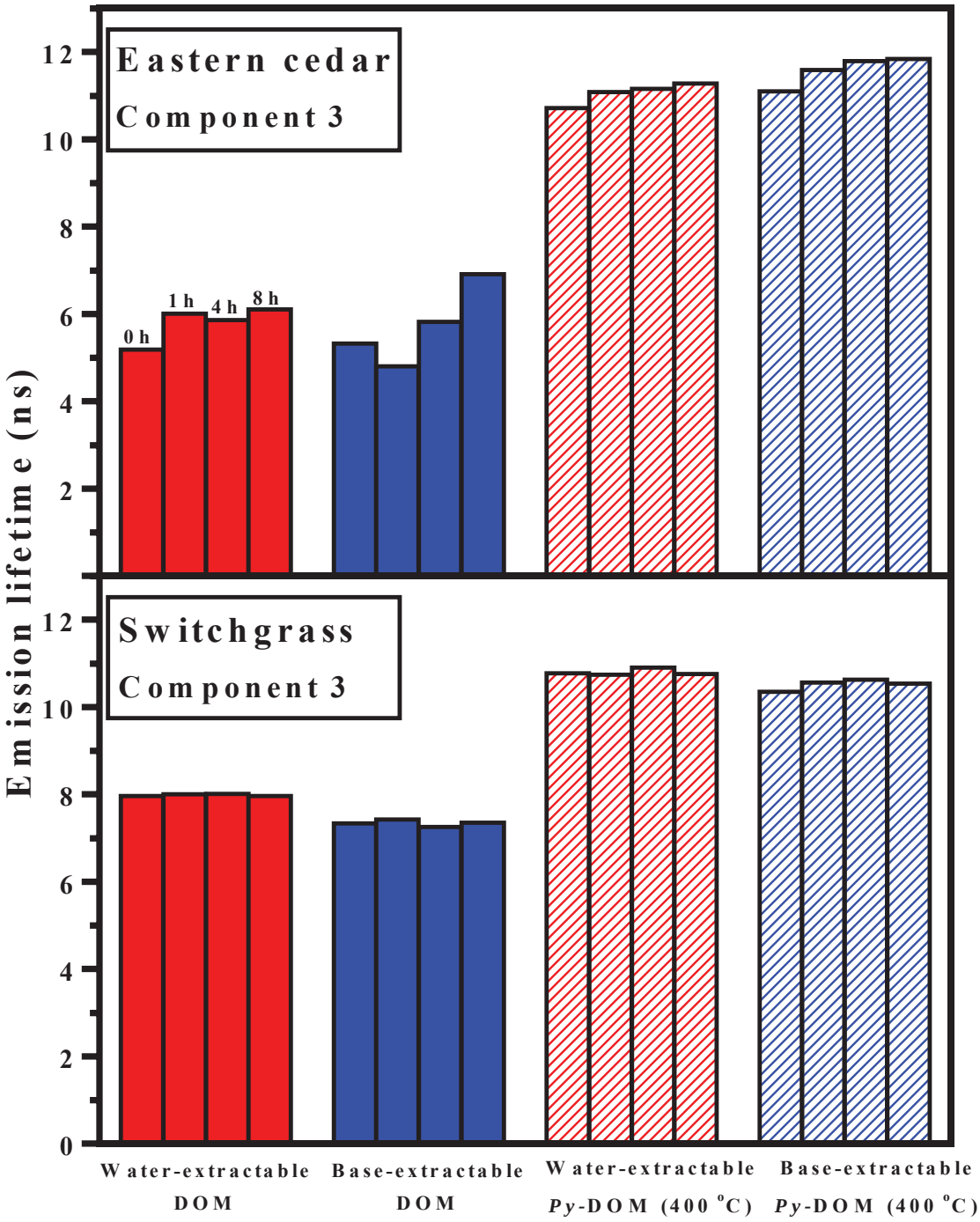

Figure 18. Component 3 lifetimes for Eastern Cedar and Switchgrass at sampling intervals of 0h, 1h, 4h, and 8h.

Table 6. Fluorescence lifetime values for DOM extracted from Eastern Cedar and Switchgrass under different heat treatment temperatures before solar exposure. All samples were excited at λ 405 nm and observed at λ 500 nm.

Materials	Parameters							
Eastern cedar	$\tau_{avg.}$ *(ns)*	τ_1 *(ns)*	α_1	τ_2 *(ns)*	α_2	τ_3 *(ns)*	α_3	χ^2
EC25	1.1	0.36±0.02	0.61±0.04	1.46±0.05	0.31±0.01	4.50±0.12	0.09±0.00	0.697
EC300	2.8	0.64±0.05	0.41±0.03	2.72±0.06	0.41±0.01	7.96±0.10	0.18±0.00	0.992
EC400	3.1	0.67±0.06	0.36±0.03	2.81±0.06	0.45±0.01	8.10±0.10	0.19±0.00	0.965
Switchgrass								
SG25	1.5	0.42±0.03	0.58±0.03	2.63±0.06	0.32±0.01	6.36±0.14	0.10±0.00	0.880
SG300	2.8	0.69±0.05	0.55±0.02	1.60±0.05	0.35±0.01	8.07±0.10	0.10±0.00	0.964
SG400	2.7	0.68±0.05	0.43±0.03	4.38±0.05	0.42±0.01	8.42±0.11	0.15±0.00	0.984
Pahokee HA	1.2	0.34±0.02	0.62±0.03	1.60±0.04	0.30±0.01	5.62±0.10	0.08	0.981

The energy-induced, component-specific responses of unpyrolyzed material agreed well with bulk fluorescence character. Trends in DOM_{deg} agreed well with α_2, suggesting that bulk changes are driven by this component. Trend in ϕ values were consistent with trends in α_3, indicative of the response of this component limiting the rate of reaction and hence kinetics of photodegradation. In unpyrolyzed samples, α_2 decreased by 56%, 22%, 37% and 3% in EC25W, SG25W, EC25B and SG25B respectively after 19.2 MJ m^{-2} energy input. During that same period α_3 decreased by 28%, 4%, 8% and 12% in EC25W, SG25W, EC25B and SG25B respectively. No loss in α_3 was observed in SG25W and EC25B prior to 19.2 MJ m^{-2}. This suggested that at least in unpyrolyzed material, component 2 was most photodegradable and component 3 had the highest contribution to the reaction rate constant. Discrepancies observed in bulk fluorescence measurements of EC25B were also observed in component lifetimes (τ_1 and τ_3) and amplitude weighted fractions (α_1 and α_3) of EC25B. In the first hour of exposure, an increase in τ_1 and a decrease in τ_3, coincided with the loss of the fluorescence emission peak centered at 520 nm, and the β region of non-linear regression curve fit. The cause of these discrepancies was unknown; however, while there was no increase in α_1 after 1 h (1.3 MJ m^{-2}), α_3 increased by 100%, thus making the α_3 component the most likely reason for those observed bulk discrepancies. Changes in α of pyrolyzed samples were not as pronounced as in unpyrolyzed samples. The most notable component-specific responses observed in pyrolyzed samples were 1) fractionable loss in α_1 after 1 h that was not observed in unpyrolyzed samples (maximum of 7% in EC400B); 2) an increase in energy input required to photodegrade α_2; and 3) minimal losses observed in α_3 with no loss observed in grass material.

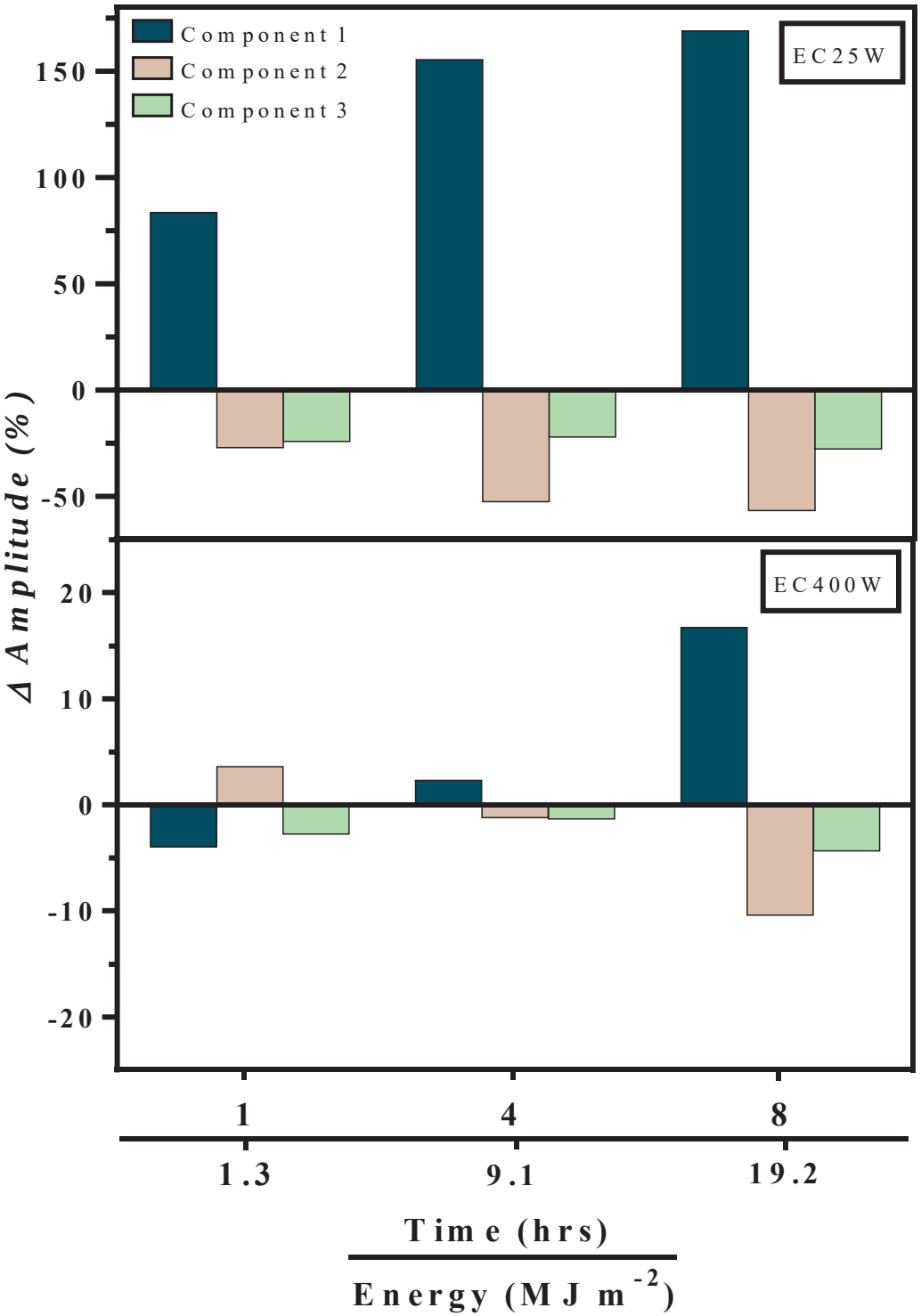

Figure 19. Effect of sunlight exposure on fluorophore population (α) of water-extracted Eastern Cedar. Note difference in *y* axis scale.

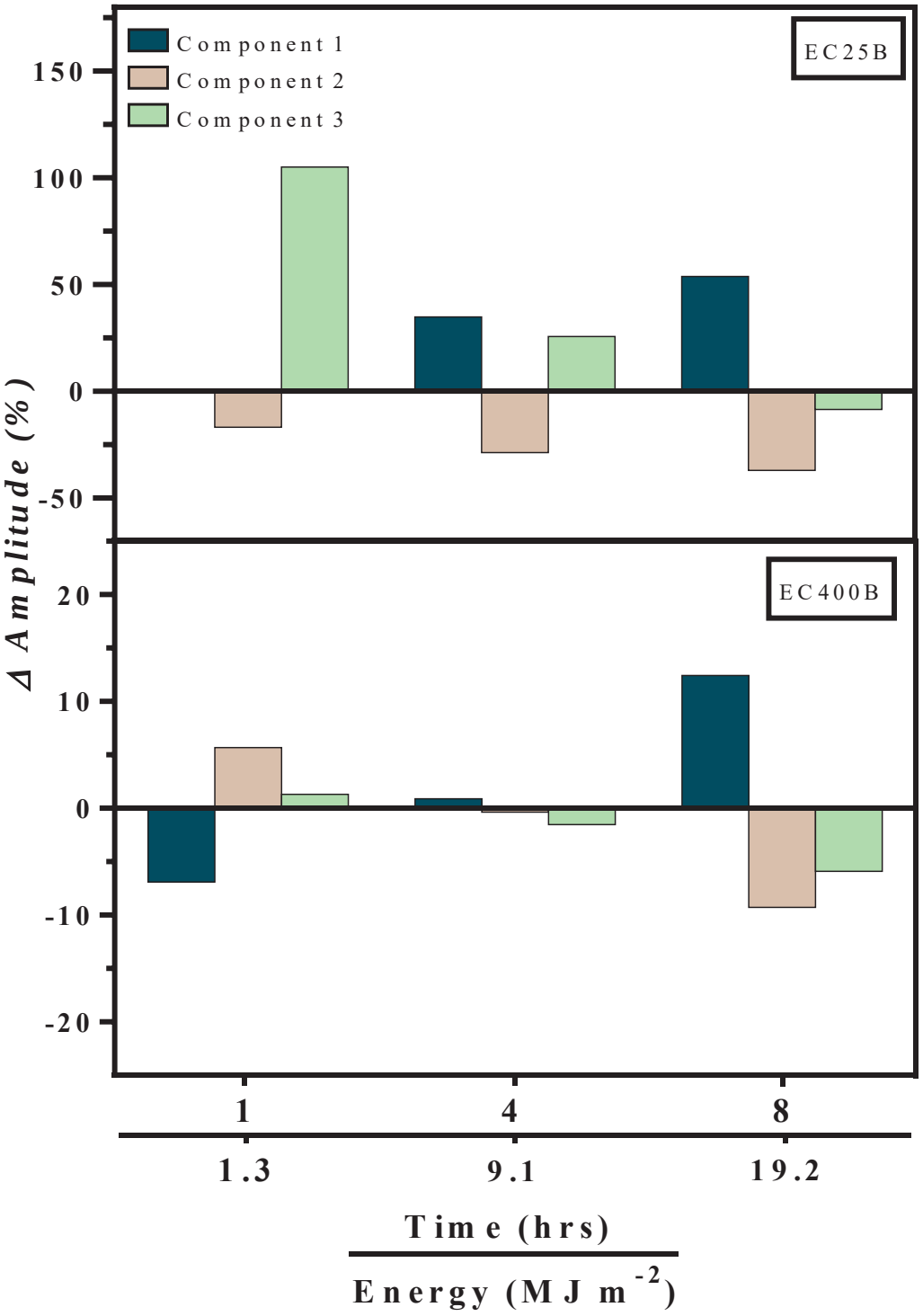

Figure 20. Effect of sunlight exposure on fluorophore population (α) of base-extracted Eastern Cedar. Note difference in *y* axis scale.

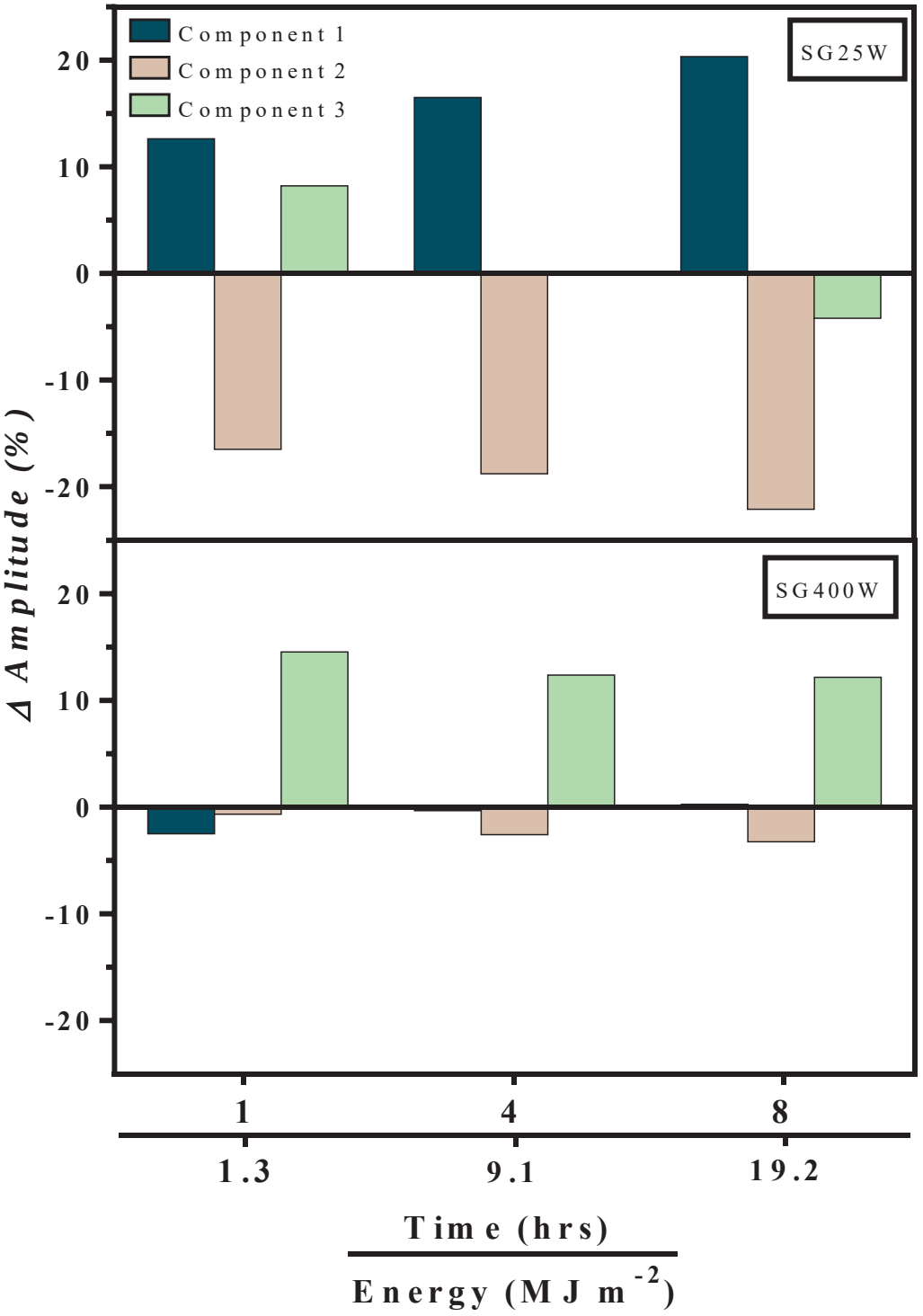

Figure 21. Effect of sunlight exposure on fluorophore population (α) water-extracted Switchgrass.

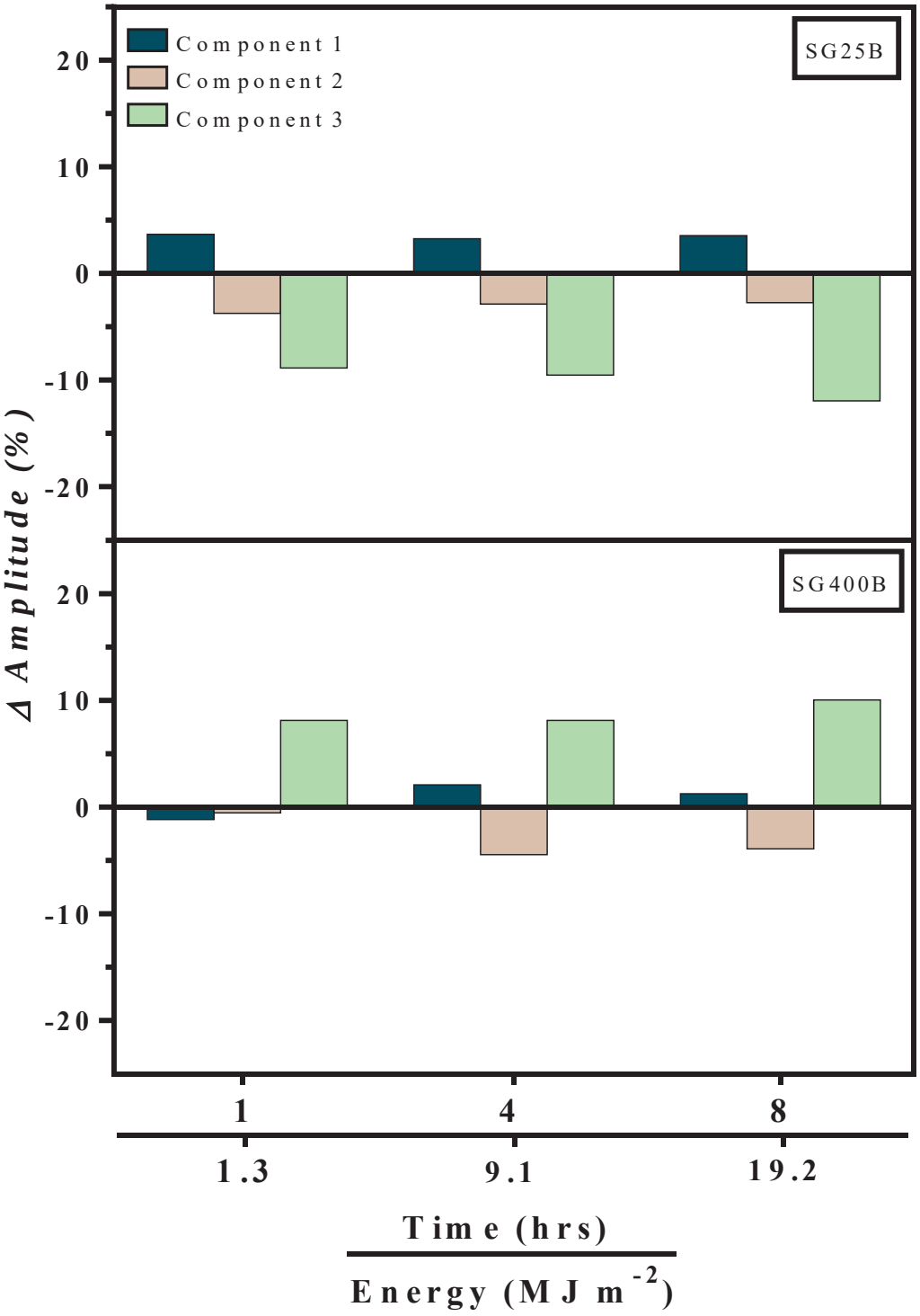

Figure 22. Effect of sunlight exposure on fluorophore population (α) of base-extracted Switchgrass.

CHAPTER III

CONCLUSIONS

Base-extracted DOM/*Py*-DOM from Eastern Cedar and Switchgrass were characterized using time-correlated single photon counting (TCSPC) and Fourier transform ion cyclotron resonance mass spectrometry (FT-ICR MS). Time-correlated single photon counting revealed a low, mid and high lifetime component similar to that observed in terrestrial aquatic and marine systems.[39] Higher molecular weight fraction and low lifetime component (τ_1) possibly represents polyaromatic lignin backbone of humic substances. Average and component lifetimes increased with increasing pyrolysis temperature; whereas fluorophore population, as indicated by amplitude weighted lifetime proportion (α), increased with pyrolysis temperature in mid and high lifetime component but decreased in low lifetime component. The principal drivers of average and component lifetimes were lignocellulose degradation products. Hence increase in fluorophore population may be attributable to cleavage of polymeric lignin phenols and levoglucosan formation, whereas carboxyl/carbonyl groups may be responsible for decrease of lifetime component.

Although it is difficult to establish the specific components driving variation in DOM vs. *Py*-DOM character, the behavior of component fractions observed using FT-ICR MS agreed well with the component fractions using lifetime spectroscopy. Unpyrolyzed material was dominated by phenolic and terpenoid compounds. Phenolic compounds in unpyrolyzed grass material dominated by cinnamyls, was more hydrogen rich than in wood material which was dominated by syringyls. Proportion of terpenoids was higher in wood versus grass material but was mostly absent from both materials upon pyrolysis. Thermal cleavage and fragmentation of long chain and/or alicyclic terpene compounds was responsible for the loss of this component and the shift of DOM to a more oxidized structure upon pyrolysis. A net-dehydration observed in both

materials upon pyrolysis shifted the molecular structure of the phenolic component to a more thermally-stable oxidized configuration. The fragmentation and net-dehydration of wood and grass material shifted the composition of samples to a carboxylic-rich alicyclic configuration with increasing pyrolysis temperature. Both wood and grass samples were comprised of a low and a high molecular weight component which decreased upon pyrolysis. However, similar MW was observed in components from pyrolyzed sample extracts suggesting that despite the alteration of the soluble component of plant material upon charring, no significant modification occurs upon further pyrolysis. This was supported by proposed molecular formulas which showed significant variation in carbon and hydrogen number upon pyrolysis, however little variation was observed between charred extracts.

In photodegradation experiments, UV-vis absorbance measurements and steady state fluorescence spectra provided a good overview of bulk characteristics of samples and changes in DOM size and structure. The *E2:E3* proxy for molecular size and aromaticity, was not found to be a robust method for tracing energy-induced changes to molecular size and/or aromaticity of samples as a function of extractant, feedstock material, and pyrolysis. The following conclusions can be made regarding bulk sample composition and the effect of energy input on bulk characteristics of DOM samples: 1) base extracts, wood feedstock, and unpyrolyzed material contained compounds of lower molecular weight/aromaticity than water extracts, grass feedstock, and pyrolyzed material respectively; 2) sunlight exposure decreased molecular weight/aromaticity in all samples; 3) degraded fraction was most dependent on feedstock material with a higher proportion of photodegradable compounds in wood than in grass material and; 4) rate of photodegradation varied highly as a function of pyrolysis in all samples and extractant in unpyrolyzed samples.

Photodegradability of lifetime components in unpyrolyzed material agreed well with ϕ and DOM_{deg} parameters obtained from I/I_0 model fit. Component 1 was most resistant and increased with energy input. Component 3 was the greatest contributor to ϕ whereas component 2 was most photodegradable. Fluorescence lifetimes of pyrolyzed material was less responsive to energy input than unpyrolyzed material, however, key differences were observed between unpyrolyzed and pyrolyzed extracts. Thermal alteration of material reduced the resistance of component 1, with minimal loss observed in all pyrolyzed samples, while component 2 and 3 showed an increased resistance to energy input.

An increase in thermally-stable oxidized products such as carboxylic-rich alicyclic molecules (CRAMS) upon pyrolysis is expected to enhance DOM interaction with ionic constituents in solution through mechanisms such as cation and anion exchange, protonation, cation-bridging, ion-pair formation and ligand exchange.[86] This highly oxidized *Py*-DOM is more resistant to microbial degradation and photodegradation than DOM. Ultimately, an increase in *Py*-DOM input in terrestrial aquatic systems points to decreased rates of carbon mineralization, and therefore a reduction in the contribution of terrestrial DOM to the deep ocean.

REFERENCES

(1) Santín, C.; Doerr, S. H.; Kane, E. S.; Masiello, C. A.; Ohlson, M.; de la Rosa, J. M.; Preston, C. M.; Dittmar, T. Towards a global assessment of pyrogenic carbon from vegetation fires. *Global Change Biology* **2016,** *22* (1), 76-91.

(2) Harvey, O. R.; Herbert, B. E.; Rhue, R. D.; Kuo, L. J. Metal interactions at the biochar-water interface: energetics and structure-sorption relationships elucidated by flow adsorption microcalorimetry. *Environmental Science Technology* **2011,** *45* (13), 5550-6.

(3) Zimmermann, M.; Bird, M. I.; Wurster, C.; Saiz, G.; Goodrick, I.; Barta, J.; Capek, P.; Santruckova, H.; Smernik, R. Rapid degradation of pyrogenic carbon. *Global Change Biology* **2012,** *18* (11), 3306-3316.

(4) Hockaday, W. C.; Grannas, A. M.; Kim, S.; Hatcher, P. G. The transformation and mobility of charcoal in a fire-impacted watershed. *Geochimica et Cosmochimica Acta* **2007,** *71* (14), 3432-3445.

(5) Kim, S.; Kaplan, L. A.; Benner, R.; Hatcher, P. G. Hydrogen-deficient molecules in natural riverine water samples—evidence for the existence of black carbon in DOM. *Marine Chemistry* **2004,** *92* (1–4), 225-234.

(6) Jaffé, R.; Ding, Y.; Niggemann, J.; Vähätalo, A. V.; Stubbins, A.; Spencer, R. G. M.; Campbell, J.; Dittmar, T. Global Charcoal Mobilization from Soils via Dissolution and Riverine Transport to the Oceans. *Science* **2013,** *340* (6130), 345-347.

(7) Moritz, M. A.; Parisien, M.-A.; Batllori, E.; Krawchuk, M. A.; Van Dorn, J.; Ganz, D. J.; Hayhoe, K., Climate change and disruptions to global fire activity. *Ecosphere* **2012,** *3* (6), 1-22.

(8) Hockaday, W. C.; Grannas, A. M.; Kim, S.; Hatcher, P. G., Direct molecular evidence for the degradation and mobility of black carbon in soils from ultrahigh-resolution mass spectral analysis of dissolved organic matter from a fire-impacted forest soil. *Organic Geochemistry* **2006,** *37* (4), 501-510.

(9) Stubbins, A.; Spencer, R. G. M.; Chen, H.; Hatcher, P. G.; Mopper, K.; Hernes, P. J.; Mwamba, V. L.; Mangangu, A. M.; Wabakanghanzi, J. N.; Six, J., Illuminated darkness: molecular signatures of Congo River dissolved organic matter and its photochemical alteration as revealed by ultrahigh precision mass spectrometry. *Limnology and Oceanography* **2010,** *55* (4), 1467-1477.

(10) Dittmar, T.; Paeng, J. A heat-induced molecular signature in marine dissolved organic matter. *Nature Geoscience* **2009,** *2* (3), 175-179.

(11) Hertkorn, N.; Benner, R.; Frommberger, M.; Schmitt-Kopplin, P.; Witt, M.; Kaiser, K.; Kettrup, A.; Hedges, J. I. Characterization of a major refractory component of marine dissolved organic matter. *Geochimica et Cosmochimica Acta* **2006,** *70*, (12) 2990-3010.

(12) Kramer, R. W.; Kujawinski, E. B.; Hatcher, P. G. Identification of black carbon derived structures in a volcanic ash soil humic acid by Fourier transform ion cyclotron resonance mass spectrometry. *Environmental Science & Technology* **2004,** *38*, 12, 3387-3395.

(13) Norwood, M. J.; Louchouarn, P.; Kuo, L.-J.; Harvey, O. R. Characterization and biodegradation of water-soluble biomarkers and organic carbon extracted from low temperature chars. *Organic Geochemistry* **2013,** *56*, 111-119.

(14) Uchimiya, M.; Hiradate, S.; Antal, M. J., Influence of carbonization methods on the aromaticity of pyrogenic dissolved organic carbon. *Energy & Fuels* **2015,** *29* (4), 2503-2513.

(15) Uchimiya, M.; Ohno, T.; He, Z. Pyrolysis temperature-dependent release of dissolved organic carbon from plant, manure, and biorefinery wastes. *Journal of Analytical and Applied Pyrolysis* **2013,** *104*, 84-94.

(16) Lin, Y.; Munroe, P.; Joseph, S.; Henderson, R.; Ziolkowski, A. Water extractable organic carbon in untreated and chemical treated biochars. *Chemosphere* **2012,** *87* (2), 151-157.

(17) Gai, X.; Wang, H.; Liu, J.; Zhai, L.; Liu, S.; Ren, T.; Liu, H., Effects of feedstock and pyrolysis temperature on biochar adsorption of ammonium and nitrate. *PLoS ONE* **2014,** *9* (12), e113888.

(18) Smith, C. R.; Sleighter, R. L.; Hatcher, P. G.; Lee, J. W., Molecular characterization of inhibiting biochar water-extractable substances using electrospray ionization Fourier transform ion cyclotron resonance mass spectrometry. *Environmental Science & Technology* **2013,** *47* (23), 13294-13302.

(19) Kuo, L. J.; Louchouarn, P.; Herbert, B. E. Influence of combustion conditions on yields of solvent-extractable anhydrosugars and lignin phenols in chars: implications for characterizations of biomass combustion residues. *Chemosphere* **2011,** *85* (5), 797-805.

(20) Smith, C. R.; Hatcher, P. G.; Kumar, S.; Lee, J. W. Investigation into the sources of biochar water-soluble organic compounds and their potential toxicity on aquatic microorganisms. *ACS Sustainable Chemistry & Engineering* **2016,** *4* (5), 2550-2558.

(21) Knicker, H.; Totsche, K. U.; Almendros, G.; González-Vila, F. J. Condensation degree of burnt peat and plant residues and the reliability of solid-state VACP MAS 13C NMR spectra obtained from pyrogenic humic material. *Organic Geochemistry* **2005,** *36* (10), 1359-1377.

(22) Stubbins, A.; Niggemann, J.; Dittmar, T. Photo-lability of deep ocean dissolved black carbon. *Biogeosciences* **2012,** *9* (5), 1661-1670.

(23) Kim, S.; Kaplan, L. A.; Hatcher, P. G. Biodegradable dissolved organic matter in a temperate and a tropical stream determined from ultra-high resolution mass spectrometry. *Limnology and Oceanography* **2006,** *51* (2), 1054-1063.

(24) Abiven, S.; Hengartner, P.; Schneider, M. P. W.; Singh, N.; Schmidt, M. W. I. Pyrogenic carbon soluble fraction is larger and more aromatic in aged charcoal than in fresh charcoal. *Soil Biology and Biochemistry* **2011,** *43* (7), 1615-1617.

(25) Ward, C. P.; Sleighter, R. L.; Hatcher, P. G.; Cory, R. M. Insights into the complete and partial photooxidation of black carbon in surface waters. *Environmental Science: Processes & Impacts* **2014,** *16* (4), 721-731.

(26) NIFC. Fire information statistics. National Interagency Fire Center, 2015; http://www.nifc.gov/fireInfo/fireInfo_statistics.html (accessed Mar 21, 2017).

(27) Santín, C.; Doerr, S. H.; Preston, C. M.; González-Rodríguez, G., Pyrogenic organic matter production from wildfires: a missing sink in the global carbon cycle. *Global Change Biology* **2015,** *21* (4), 1621-1633.

(28) Zimmerman, A. R., Abiotic and microbial oxidation of laboratory-produced black carbon (biochar). *Environmental Science & Technology* **2010,** *44* (4), 1295-1301.

(29) Fang, Y.; Singh, B.; Singh, B. P.; Krull, E. Biochar carbon stability in four contrasting soils. *European Journal of Soil Science* **2014,** *65* (1), 60-71.

(30) Kuzyakov, Y.; Bogomolova, I.; Glaser, B. Biochar stability in soil: decomposition during eight years and transformation as assessed by compound-specific 14C analysis. *Soil Biology and Biochemistry* **2014,** *70*, 229-236.

(31) Novotny, E. H.; Auccaise, R.; Lima, L. B.; Madari, B. E. Characterisation of humic substances extracted from soil treated with charcoal (biochar). In *Functions of Natural Organic Matter in Changing Environment*; Xu, J.; Wu, J.; He, Y., Eds.; Springer Netherlands: Dordrecht, 2013; pp 971-974.

(32) Kujawinski, E. B.; Hatcher, P. G.; Freitas, M. A. High-resolution fourier transform ion cyclotron resonance mass spectrometry of humic and fulvic acids: improvements and comparisons. *Analytical Chemistry* **2002,** *74* (2), 413-419.

(33) Myers-Pigg, A. N.; Louchouarn, P.; Amon, R. M. W.; Prokushkin, A.; Pierce, K.; Rubtsov, A. Labile pyrogenic dissolved organic carbon in major Siberian Arctic rivers: implications for wildfire-stream metabolic linkages. *Geophysical Research Letters* **2015,** *42* (2), 377-385.

(34) Clifford, D. J.; Carson, D. M.; McKinney, D. E.; Bortiatynski, J. M.; Hatcher, P. G. A new rapid technique for the characterization of lignin in vascular plants: thermochemolysis with tetramethylammonium hydroxide (TMAH). *Organic Geochemistry* **1995,** *23* (2), 169-175.

(35) Arakawa, N.; Aluwihare, L. Direct identification of diverse alicyclic terpenoids in Suwannee River Fulvic Acid. *Environmental Science & Technology* **2015,** *49* (7), 4097-4105.

(36) Sleighter, R. L.; Hatcher, P. G. The application of electrospray ionization coupled to ultrahigh resolution mass spectrometry for the molecular characterization of natural organic matter. *Journal of Mass Spectrometry* **2007,** *42* (5), 559-574.

(37) Riedel, T.; Iden, S.; Geilich, J.; Wiedner, K.; Durner, W.; Biester, H. Changes in the molecular composition of organic matter leached from an agricultural topsoil following addition of biomass-derived black carbon (biochar). *Organic Geochemistry* **2014,** *69*, 52-60.

(38) Markechová, D.; Tomková, M.; Sádecká, J. Fluorescence excitation-emission matrix spectroscopy and parallel factor analysis in drinking water treatment: a review. *Polish Journal of Environmental Studies* **2013,** *22* (5), 1289-1295.

(39) Clark, C. D.; Jimenez-Morais, J.; Jones Ii, G.; Zanardi-Lamardo, E.; Moore, C. A.; Zika, R. G. A time-resolved fluorescence study of dissolved organic matter in a riverine to marine transition zone. *Marine Chemistry* **2002,** *78* (2–3), 121-135.

(40) Boyle, E. S.; Guerriero, N.; Thiallet, A.; Del Vecchio, R.; Blough, N. V. Optical properties of humic substances and CDOM: relation to structure. *Environmental Science & Technology* **2009,** *43* (7), 2262-2268.

(41) Olk, D. C.; Gregorich, E. G. Overview of the symposium proceedings, "Meaningful pools in determining soil carbon and nitrogen dynamics". *Soil Science Society of America Journal* **2006,** *70* (3), 967-974.

(42) Thurman, E. M.; Malcolm, R. L. Preparative isolation of aquatic humic substances. *Environmental Science & Technology* **1981,** *15* (4), 463-466.

(43) NADP. Hydrogen ion concentration as pH from measurements made at the Central Analytical Laboratory. National Atmospheric Deposition Program, 2015; http://nadp.sws.uiuc.edu/ (accessed Mar 21, 2017).

(44) Dittmar, T.; Koch, B.; Hertkorn, N.; Kattner, G. A simple and efficient method for the solid-phase extraction of dissolved organic matter (SPE-DOM) from seawater. *Limnology and Oceanography: Methods* **2008,** *6* (6), 230-235.

(45) Kujawinski, E. B.; Behn, M. D. Automated analysis of electrospray ionization Fourier transform ion cyclotron resonance mass spectra of natural organic matter. *Anal. Chem.* **2006,** *78* (13), 4363-4373.

(46) Kujawinski, E. B. Electrospray ionization fourier transform ion cyclotron resonance mass spectrometry (ESI FT-ICR MS): characterization of complex environmental mixtures. *Environmental Forensics* **2002,** *3* (3), 207-216.

(47) Coble, P. G. Marine optical biogeochemistry: the chemistry of ocean color. *Chemical Reviews* **2007,** *107* (2), 402-418.

(48) Baker, A.; Spencer, R. G. M. Characterization of dissolved organic matter from source to sea using fluorescence and absorbance spectroscopy. *Science of The Total Environment* **2004,** *333* (1–3), 217-232.

(49) Coble, P. G. Characterization of marine and terrestrial DOM in seawater using excitation-emission matrix spectroscopy. *Marine Chemistry* **1996,** *51* (4), 325-346.

(50) Sutton, R.; Sposito, G. Molecular structure in soil humic substances: the new view. *Environmental Science & Technology* **2005,** *39* (23), 9009-9015.

(51) Stenson, A. C.; Marshall, A. G.; Cooper, W. T. Exact masses and chemical formulas of individual Suwannee River Fulvic Acids from ultrahigh resolution electrospray ionization Fourier transform ion cyclotron resonance mass spectra. *Analytical Chemistry* **2003,** *75* (6), 1275-1284.

(52) Rutherford, D. W.; Wershaw, A. L.; Reeves, J. B. I. Development of acid functional groups and lactones during the thermal degradation of wood and wood components. *United States Geological Survey Scientific Investigations report* **2007,** 2007-5013.

(53) Kuhnert, N.; Dairpoosh, F.; Yassin, G.; Golon, A.; Jaiswal, R. What is under the hump? Mass spectrometry based analysis of complex mixtures in processed food - lessons from the characterisation of black tea thearubigins, coffee melanoidines and caramel. *Food & Function* **2013,** *4* (8), 1130-1147.

(54) Hertkorn, N.; Frommberger, M.; Witt, M.; Koch, B. P.; Schmitt-Kopplin, P.; Perdue, E. M. Natural organic matter and the event horizon of mass spectrometry. *Analytical Chemistry* **2008,** *80* (23), 8908-8919.

(55) Willoughby, A. S.; Wozniak, A. S.; Hatcher, P. G. A molecular-level approach for characterizing water-insoluble components of ambient organic aerosol particulates using ultrahigh-resolution mass spectrometry. *Atmospheric Chemistry and Physics.* **2014,** *14* (18), 10299-10314.

(56) Lu, Y.; Li, X.; Mesfioui, R.; Bauer, J. E.; Chambers, R. M.; Canuel, E. A.; Hatcher, P. G. Use of ESI-FTICR-MS to characterize dissolved organic matter in headwater streams draining forest-dominated and pasture-dominated watersheds. *PLoS One* **2015,** *10* (12), e0145639.

(57) Baldock, J. A.; Smernik, R. J. Chemical composition and bioavailability of thermally altered Pinus resinosa (Red pine) wood. *Organic Geochemistry* **2002,** *33* (9), 1093-1109.

(58) Hammes, K.; Smernik, R. J.; Skjemstad, J. O.; Herzog, A.; Vogt, U. F.; Schmidt, M. W. I. Synthesis and characterisation of laboratory-charred grass straw (Oryza sativa) and chestnut wood (Castanea sativa) as reference materials for black carbon quantification. *Organic Geochemistry* **2006,** *37* (11), 1629-1633.

(59) Minor, E. C.; Steinbring, C. J.; Longnecker, K.; Kujawinski, E. B. Characterization of dissolved organic matter in Lake Superior and its watershed using ultrahigh resolution mass spectrometry. *Organic Geochemistry* **2012,** *43*, 1-11.

(60) Podgorski, D. C.; Hamdan, R.; McKenna, A. M.; Nyadong, L.; Rodgers, R. P.; Marshall, A. G.; Cooper, W. T. Characterization of pyrogenic black carbon by desorption atmospheric pressure photoionization Fourier transform ion cyclotron resonance mass spectrometry. *Analytical Chemistry* **2012,** *84* (3), 1281-1287.

(61) Keeling, C. I.; Bohlmann, J. Diterpene resin acids in conifers. *Phytochemistry* **2006,** *67* (22), 2415-2423.

(62) Pinene. In *The Merck Index - An encyclopedia of chemicals, drugs, and biologicals.;* Merck and Co., Inc: New Jersey, 2006; pp. 1283.

(63) Dewick, P. M. The biosynthesis of C5-C25 terpenoid compounds. *Natural Product Reports* **2002,** *19* (2), 181-222.

(64) Lam, B.; Baer, A.; Alaee, M.; Lefebvre, B.; Moser, A.; Williams, A.; Simpson, A. J. major structural components in freshwater dissolved organic matter. *Environmental Science & Technology* **2007,** *41* (24), 8240-8247.

(65) Harvey, O. R.; Herbert, B. E.; Kuo, L.-J.; Louchouarn, P. Generalized two-dimensional perturbation correlation infrared spectroscopy reveals mechanisms for the development of surface charge and recalcitrance in plant-derived biochars. *Environmental Science & Technology* **2012,** *46* (19), 10641-10650.

(66) Yang, H.; Yan, R.; Chen, H.; Lee, D. H.; Zheng, C. Characteristics of hemicellulose, cellulose and lignin pyrolysis. *Fuel* **2007,** *86* (12–13), 1781-1788.

(67) Ramachandriya, K. D.; Wilkins, M.; Pardo-Planas, O.; Atiyeh, H. K.; Dunford, N. T.; Hiziroglu, S. Simultaneous saccharification and fermentation of Eastern redcedar heartwood and sapwood using a novel size reduction technique. *Bioresource Technology* **2014,** *161*, 1-9.

(68) Ververis, C.; Georghiou, K.; Christodoulakis, N.; Santas, P.; Santas, R. Fiber dimensions, lignin and cellulose content of various plant materials and their suitability for paper production. *Industrial Crops and Products* **2004,** *19* (3), 245-254.

(69) Leenheer, J. A.; Nanny, M. A.; McIntyre, C. Terpenoids as major precursors of dissolved organic matter in landfill leachates, surface water, and groundwater. *Environmental Science & Technology* **2003,** *37* (11), 2323-2331.

(70) Roth, V.-N.; Dittmar, T.; Gaupp, R.; Gleixner, G. The molecular composition of dissolved organic matter in forest soils as a function of pH and temperature. *PLoS ONE* **2015,** *10* (3), e0119188.

(71) Mukherjee, A.; Zimmerman, A. R.; Harris, W. Surface chemistry variations among a series of laboratory-produced biochars. *Geoderma* **2011,** *163* (3–4), 247-255.

(72) Nguyen, B. T.; Lehmann, J. Black carbon decomposition under varying water regimes. *Organic Geochemistry* **2009,** *40* (8), 846-853.

(73) McBeath, A. V.; Wurster, C. M.; Bird, M. I. Influence of feedstock properties and pyrolysis conditions on biochar carbon stability as determined by hydrogen pyrolysis. *Biomass and Bioenergy* **2015,** *73*, 155-173.

(74) Hedges, J. I.; Eglinton, G.; Hatcher, P. G.; Kirchman, D. L.; Arnosti, C.; Derenne, S.; Evershed, R. P.; Kögel-Knabner, I.; de Leeuw, J. W.; Littke, R.; Michaelis, W.; Rullkötter, J. The molecularly-uncharacterized component of nonliving organic matter in natural environments. *Organic Geochemistry* **2000,** *31* (10), 945-958.

(75) Santos, F.; Torn, M. S.; Bird, J. A. Biological degradation of pyrogenic organic matter in temperate forest soils. *Soil Biology and Biochemistry* **2012,** *51*, 115-124.

(76) Kuzyakov, Y.; Subbotina, I.; Chen, H.; Bogomolova, I.; Xu, X. Black carbon decomposition and incorporation into soil microbial biomass estimated by 14C labeling. *Soil Biology and Biochemistry* **2009,** *41* (2), 210-219.

(77) Helms, J. R.; Stubbins, A.; Ritchie, J. D.; Minor, E. C.; Kieber, D. J.; Mopper, K. Absorption spectral slopes and slope ratios as indicators of molecular weight, source, and photobleaching of chromophoric dissolved organic matter. *Limnology and Oceanography* **2008,** *53* (3), 955-969.

(78) Lechtenfeld, O. J.; Kattner, G.; Flerus, R.; McCallister, S. L.; Schmitt-Kopplin, P.; Koch, B. P. Molecular transformation and degradation of refractory dissolved organic matter in the Atlantic and Southern Ocean. *Geochimica et Cosmochimica Acta* **2014,** *126*, 321-337.

(79) Dittmar, T.; de Rezende, C. E.; Manecki, M.; Niggemann, J.; Coelho Ovalle, A. R.; Stubbins, A.; Bernardes, M. C. Continuous flux of dissolved black carbon from a vanished tropical forest biome. *Nature Geoscience* **2012,** *5* (9), 618-622.

(80) Ding, Y.; Yamashita, Y.; Jones, J.; Jaffé, R. Dissolved black carbon in boreal forest and glacial rivers of central Alaska: assessment of biomass burning versus anthropogenic sources. *Biogeochemistry* **2014,** *123* (1), 15-25.

(81) Mannino, A.; Harvey, H. R. Black carbon in estuarine and coastal ocean dissolved organic matter. *Limnology and Oceanography* **2004,** *49* (3), 735-740.

(82) Dittmar, T.; Paeng, J.; Gihring, T. M.; Suryaputra, I. G. N. A.; Huettel, M. Discharge of dissolved black carbon from a fire-affected intertidal system. *Limnology and Oceanography* **2012,** *57* (4), 1171-1181.

(83) Rajca, M.; Bodzek, M. Kinetics of fulvic and humic acids photodegradation in water solutions. *Separation and Purification Technology* **2013,** *120*, 35-42.

(84) NREL. US solar resource map. National Renewable Energy Laboratory, 2008; http://www.nrel.gov/gis/solar.html (accessed Mar 21, 2017).

(85) He, W.; Lee, J.-H.; Hur, J. Anthropogenic signature of sediment organic matter probed by UV–visible and fluorescence spectroscopy and the association with heavy metal enrichment. *Chemosphere* **2016,** *150*, 184-193.

(86) Ohno, T. Fluorescence inner-filtering Correction for determining the humification index of dissolved organic matter. *Environmental Science & Technology* **2002,** *36* (4), 742-746.

VITA

Personal Background
Burke Chadfield Leonce
Castries, Saint Lucia
Son of Maurice Jn Baptiste and Barbara Jn Baptiste
Married Shermaye Khadiya Nelson, December 10, 2016

Education
2006 A level Certificate, Sir Arthur Lewis Community College, Castries, Saint Lucia

2010 Bachelor of Science, Environmental Science, Troy University, Troy, Alabama

2017 Master of Science, Environmental Science, Texas Christian University, Fort Worth, Texas

Experience
Teacher, Vide Bouteille Secondary School, Castries, Saint Lucia, 2006-2007

Academic Support Specialist, El Puente Leadership Center, Brooklyn, New York, 2010-2011

Asbestos Laboratory Technician, EMSL Analytical Inc, New York, New York, 2011-2012

Zonal Supervisor, Saint Lucia Solid Waste Management Authority, Castries, St. Lucia, 2012-2015

Teaching Assistant, Texas Christian University, Fort Worth, Texas, 2015-2017

Presentations
Leonce, B.C., and O.R. Harvey. 2016. "Ion-Probe Flow-Adsorption Microcalorimetry: A New Approach to the Study of Surface Heterogeneity, Acid Dissociation and Cation Exchange Behavior at the *Py*C-Water Interface." 251st American Chemical Society National Meeting & Exposition. San Diego Ca.

Leonce, B.C. 2016. "When the smoke clears – How clean is your water?" Texas Christian University Three Minute Thesis (3MT) Competition. Fort Worth, TX

ABSTRACT

PHOTODEGRADATION OF PYROGENIC DISSOLVED ORGANIC MATTER (*PY*-DOM): A COMBINED PHOTON COUNTING AND DISTRIBUTION-BASED FT-ICR MS STUDY

by Burke C. Leonce, M.S., 2017
School of Geology, Energy, and the Environment
Texas Christian University

Thesis Advisor: Omar Harvey, Associate Professor of Environmental Science

Quantitative systematic studies are needed to elucidate the both short and long-term environmental implications of increasing pyrogenic dissolved organic matter (*Py*-DOM) inputs associated with projected increase in wildfire activity over the next century. Time-resolved fluorescence spectroscopy and Fourier transform ion cyclotron resonance were used to characterize extracts of unaltered and pyrolyzed wood and plant material. Upon pyrolysis, extracts shifted from a predominantly phenolic signature to a carboxylic-rich alicyclic configuration. Photodegradation of extracts was commensurate with solar energy exposure. The rate of photodegradation and the degradable fraction of DOM was component driven. Results of this study point to a disproportionate energy-induced response in components common to lignocellulose-derived DOM. Further studies are required to elucidate the mechanistic aspect of photodegradation of DOM, and *Py*-DOM as relates to energy input.